Quaternary International xxx (2016) 1–15

Contents lists available at ScienceDirect

Quaternary International

journal homepage: www.elsevier.com/locate/quaint

Climate change evidences from the end of the Little Ice Age to the Current Warm Period registered by Melincué Lake (Northern Pampas, Argentina)

Lucía Guerra [a, *], Eduardo L. Piovano [a], Francisco E. Córdoba [b], Kazuyo Tachikawa [c], Frauke Rostek [c], Marta Garcia [c], Edouard Bard [c], Florence Sylvestre [c]

[a] Centro de Investigaciones en Ciencias de la Tierra (CICTERRA, CONICET-Universidad Nacional de Córdoba), Ciudad Universitaria, Av. Vélez Sarsfield 1611, X5016GCA, Córdoba, Argentina
[b] Centro de Investigación y Transferencia de Jujuy (CIT, Jujuy-CONICET), Instituto de Geología y Minería, Universidad Nacional de Jujuy, Av. Bolivia, 1661, San Salvador de Jujuy, Argentina
[c] Aix-Marseille Université, CNRS, IRD, Collège de France, UM34 CEREGE, Technopôle de l'Environnement Arbois-Méditerranée, BP80, 13545 Aix-en-Provence, France

ARTICLE INFO

Article history:
Available online xxx

Keywords:
Argentinean Pampean lakes
Lacustrine sediments
X-ray fluorescence
South American Monsoon
Current Warm Period

ABSTRACT

Geochemical, sedimentological, historical and instrumental information from Melincué Lake (33°43′S/61°28′W) was analyzed in order to reconstruct main hydro-climatic changes along the Pampean region, considering the end of the Little Ice Age (LIA) and the Current Warm Period (CWP) climatic phases. Elemental X-ray fluorescence determinations were performed on a dated short core extracted from the deepest part of the lake. Chemical (Ca, Sr, Al, K, Si, Ti and Fe) variation was analyzed along with physical (magnetic susceptibility, dry bulk density and medium particle size) and mineralogical proxies, as well as carbon and nitrogen contents (organic and inorganic carbon and organic nitrogen). Multicomponent statistical analyses allowed the identification of the main environmental processes ruling sedimentation, which included carbonate precipitation, detrital input and primary productivity. Homogeneous, carbonate-rich, detrital-rich and organic matter-poor deposits reflect very shallow and ephemeral lake conditions during the last years of the LIA period. Very low sedimentation rates and the presence of discontinuities in the sedimentary record pointed to episodes of extensive lake shrinkages and probable lake-floor subaerial exposures. Bedded and laminated organic-rich muds accumulated in perennial lake conditions after ca. AD 1880 reveal an important environmental change concurrent with the onset of the Current Warm Period. The contrast of sediment composition and lithological characteristics with the instrumental record of the CWP allowed us to consider the development of a shallow saline-lake system, enhanced detrital input and carbonate precipitation during dry periods. In turn, higher lake levels, and thus more diluted lake-waters during wetter periods, resulted in enhanced organic lake productivity and lower carbonate precipitation. The comparison of the paleolimnological reconstruction from Melincué Lake to different hydrological and paleoclimatic records (i.e. limnimetric measurements and ocean temperature changes) suggests that the moisture variation registered between the LIA and the CWP was consistent with (and likely forced by) large-scale climatic oscillations. The present study provides new evidences to evaluate the climate and environmental changes in central Argentina related to the dynamics of the South American Monsoon system during the last five centuries.

© 2016 Elsevier Ltd and INQUA. All rights reserved.

Abbreviations: LIA, Little Ice Age; CWP, current warm period; CRS, Constant Rate of Supply; SAM, South American Monsoon; SACZ, South Atlantic Convergence Zone; SALLJ, South American Low Level Jet; SESA, Southeastern South America; ENSO, El Niño Southern Oscillation; MS, magnetic susceptibility; TOC, total organic carbon; TIC, total inorganic carbon; TN, total nitrogen.; PCA, principal component analysis; PC, principal component; RPI, Regional Precipitation Index; SST, sea surface temperature.

* Corresponding author.
E-mail address: luciaguerra83@gmail.com (L. Guerra).

http://dx.doi.org/10.1016/j.quaint.2016.06.033
1040-6182/© 2016 Elsevier Ltd and INQUA. All rights reserved.

Please cite this article in press as: Guerra, L., et al., Climate change evidences from the end of the Little Ice Age to the Current Warm Period registered by Melincué Lake (Northern Pampas, Argentina), Quaternary International (2016), http://dx.doi.org/10.1016/j.quaint.2016.06.033

1. Introduction

The Argentine Pampean Plain is a key area to examine late Holocene hydroclimatic changes in the Southern Hemisphere. In spite of the increasing number of paleoclimatic reconstructions and model simulations of regional climate variability in South America, they are mostly focused on the western and southern area (e.g. Mann et al., 2009; Neukom et al., 2011, 2014) with much uncertainty the southeastern portion of the continent, which includes the Pampas in central-east Argentina. This is the most populated area of Argentina, where the socio-economical activities strongly rely on the water resources and therefore, on hydrological changes. The climate of the Pampean region is defined by the superposition of short and long term fluctuations of the South American Monsoon (SAM) activity and the Pacific and Atlantic ocean-atmosphere dynamics (Garreaud et al., 2009). Recent and past SAM regional variability can be traced through a combined analysis of instrumental, historical and high-resolution climate records.

Multiple paleoclimatological studies in the sedimentary record of fluvial, lacustrine, soil and aeolian sequences along the Pampean plain (e.g. Cioccale, 1999; Kröhling, 1999; Kröhling and Iriondo, 1999; Zárate, 2003; Iriondo et al., 2009; Stutz et al., 2012; Tripaldi et al., 2013; Piovano et al., 2014) revealed significant environmental changes during the late Holocene. For instance, several reconstructions indicate dominant arid and cold conditions in the Little Ice Age (LIA, AD 1500–1850; Bradley et al., 2003; Jones and Mann, 2004) across the Argentinean Pampas (Cioccale, 1999; Kröhling and Iriondo, 1999; Tonni et al., 1999; Piovano et al., 2002; 2004; Deschamps and Tonni, 2007; Iriondo and Kröhling, 2007). The LIA was not uniform and two main pulses were recognized, the first one between the 14th and 15th centuries, and the second and coldest during the first half of the 19th century (Villalba, 1994; Cioccale, 1999; PAGES 2k Consortium, 2013; McGregor et al., 2015). A temperature increase starting towards the end of the 19th century marks the onset of the Current Warm Period (CWP, AD, 1850/1900-present day; Bird et al., 2011; Thompson et al., 2013). Subsequently, the first decades of the 20th century were characterized by low river discharges and lake-levels across southeastern South America. This dry stage was followed by a extremely humid period which extended from the beginning and middle 1970s until 2003 (Giorgi, 2002; Pasquini et al., 2006; Piovano et al., 2009; Troin et al., 2010, 2015; Córdoba et al., 2014).

The timing and frequency of late Holocene climate changes across the Pampean Plains and their relation with large-scale circulation patterns in southeastern South America are not completely resolved. Thus, shallow lakes located in the humid Pampas provide a broad collection for deciphering sedimentary records of climatic unevenness during the late Holocene, including the LIA and the CWP (Piovano et al., 2009; Stutz et al., 2012; Córdoba et al., 2014; Laprida et al., 2014a,b, among others). Particularly, the LIA-CWP transition record from Pampean terrestrial aquatic systems show a wide-spread and gradual hydrological changes from ephemeral saline lakes and playa complexes into perennial lake-systems as a consequence of comparatively more positive precipitation-evaporation balances (Córdoba et al., 2014; Guerra et al., 2015). Although the area was initially occupied by aboriginal people probably since 10,000 years BP, several villages were founded by Europeans immigrants during the end of the 19th century, matching the LIA-CWP transition. Very low lake levels likely forced settlement close to the lakes, usually below the topographic levels of geomorphological evidences of former high-stands (Leroy et al., 2010). The 20th century pulses of Pampean lakes' expansion-retraction impacted on the infrastructure and local economy of villages settled by the lakes' shores, especially during the humid pulse recorded between 1970s and 2003 (Leroy et al., 2010; Piovano et al., 2014). At a regional scale, this wet phase impacted on traditional socio-economy of a densely populated area of Argentina, which strongly relies on the water resources and is highly susceptible to hydrological unevenness (Leroy et al., 2010). After year 2003, the instrumental water-lake level records of Pampean lakes (Mar Chiquita Lake 30°S/62°W, Melincué Lake 33°S/61°W, Lagunas Encadenadas del Oeste de Buenos Aires 37°S/62°W; see Córdoba et al., 2014; Fig. 1a) showed a dramatic fall following regional drier conditions up to year 2014, when an hydrological reverse (higher lake levels and precipitations) started.

Previous results have shown the potential of Melincué lacustrine sedimentary archive for analyzing past regional environmental changes in the Pampean Plains (Guerra, 2015; Guerra et al., 2015). The sedimentological facies allowed reconstructing alternating lake expansions and retractions over the last millennium as the result of changes in regional precipitation over the Pampean region.

In this contribution we employ a combined analysis of sedimentological and petro-physical data with geochemical information (X-Ray Fluorescence) of a previously dated sedimentary core from Melincué Lake to better-understand the sedimentation processes and the lake response during contrasting climatic phases. Focusing the analysis on the last part of the LIA and the CWP, we compare the obtained limnogeological reconstruction with local (i.e. instrumental water lake-level) and regional hydroclimatic variables (i.e. regional precipitation indices, RPI). We then inspect the reconstructed lake variability over a larger spatial-scale perspective, contrasting our results with other well-studied ocean-temperature reconstructions affecting South American climate. The results of this research contribute to disentangle the behavior and the role of the South American Monsoon activity on the past climate variability in its southernmost influence area.

2. Regional setting

Melincué Lake (33° 43′S/61°28′ W; Fig. 1a) is a shallow (4.25 m maximum depth), hydrologically closed system. It is an underfilled to balance-filled (i.e. oscillating between alkaline and freshwater, with progradation and aggradation; Carroll and Bohacs, 1999) lake basin located within a structural depression in the eastern Argentinean Pampean Plains (Pasotti et al., 1984; Brunetto et al., 2010; Dávila et al., 2010) associated with the southern part of the Tostado-Selva Fault System and the San Guillermo Elevated Block, generated by neotectonics (Kröhling, 1999; Brunetto et al., 2010). The origin of the lake can be linked to a structural sinking of a small block inside the main depression, and a subsequent damming of the paleo-drainage system which had previously flown in a SW–NE direction (Pasotti et al., 1984; Iriondo and Kröhling, 2007). The lacustrine basin is surrounded by aeolian loess, loessoid (Peripheral Loess Belt; Iriondo and Kröhling, 2007), composed of feldspars (plagioclase and K-feldespars), quartz, illite, kaolinite, and volcanic glass, from the Tezanos Pinto and San Guillermo Formations (Kemp et al., 2004), and palustrine sediments from the Pleistocene and Holocene (Kröhling, 1999; Fig. 1b).

The lake is fed by unconfined outwash, a permanent stream -El Pedernal (Fig. 1c) – and phreatic groundwater inputs (Pasotti et al., 1984). Currently, the catchment area is 680 km^2, the water body occupies ~62 km^2 and the maximum water-depth is around 4.3 m (Fig. 1c). Lake water is alkaline with a pH > 9, subsaline (TDS > 2000 ppm) and its composition is currently dominated by Na^+ and HCO_3^-. Nevertheless, the closed-lake setting coupled with gentle slopes result in significant variability of the lake area, the water composition, and also of the spatial distributions of sub-environments during lake level fluctuations (Fig. 1d). For

Please cite this article in press as: Guerra, L., et al., Climate change evidences from the end of the Little Ice Age to the Current Warm Period registered by Melincué Lake (Northern Pampas, Argentina), Quaternary International (2016), http://dx.doi.org/10.1016/j.quaint.2016.06.033

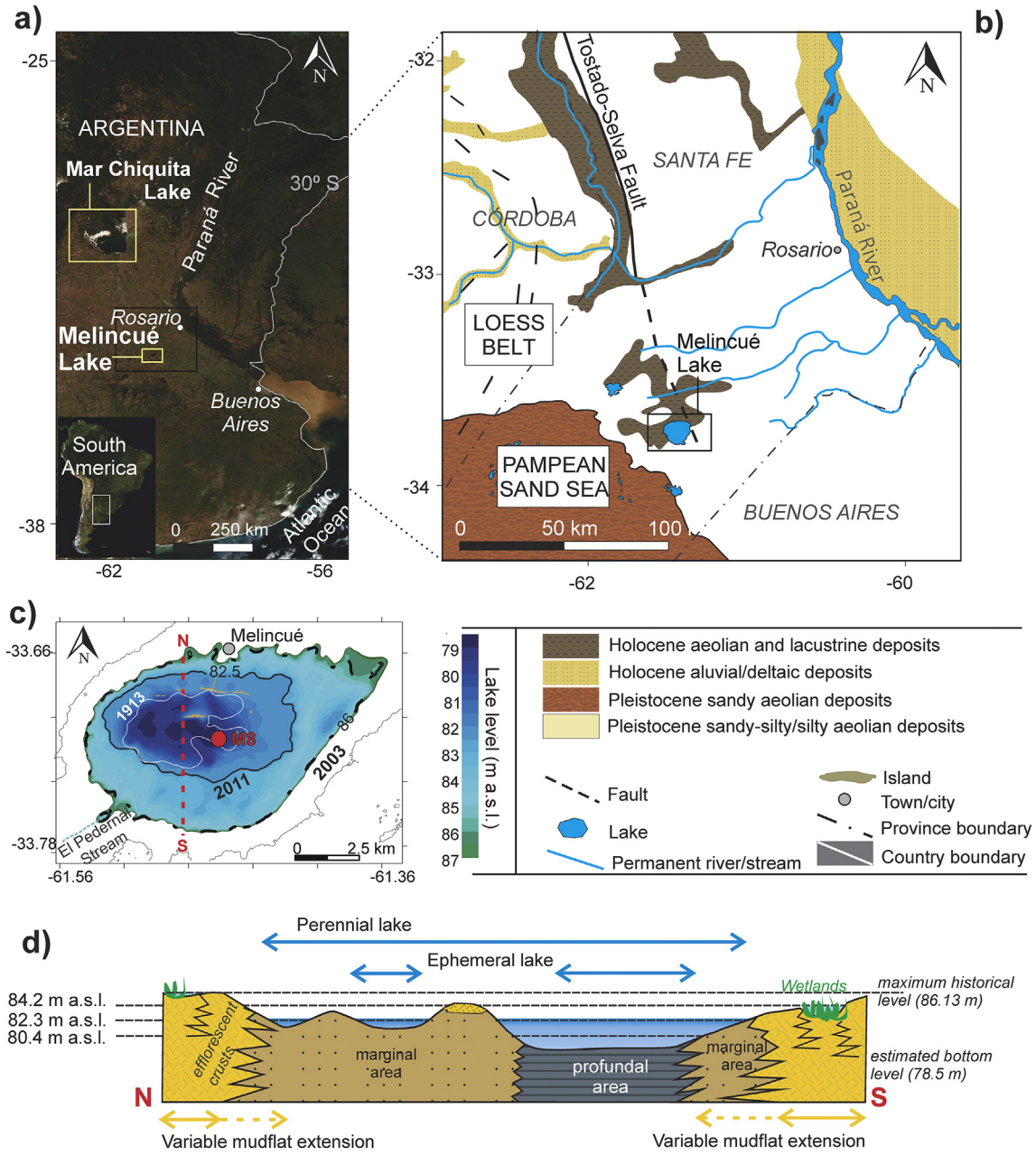

Fig. 1. General setting of the study site. **a)** Satellite image and location of the Melincué Lake (Blue Marble, NASA Earth Observatory). **b)** Geology and sedimentary deposits of the study area within the Pampean Region (taken from Guerra et al., 2015; modified from the Servicio Geológico Minero, 1997); Melincué Lake is located within the Loess Belt of the Pampean Aeolian System (Iriondo and Kröhling, 1995), inside a N–S depression limited by the Tostado-Selva fault (Pasotti and Castellanos, 1963). **c)** Contour map highlighting the lake levels in 2003 (dashed line), 2011 (continuous dark line) and 1913 (continuous white line; Pasotti et al., 1984). The circle indicates the position of M8 core, retrieved in 2011. **d)** N–S schematic topographic profile (its position on the lake is indicated in c) as a dashed line, showing the main depositional sub-environments and their variation according to the lake level state from ephemeral to perennial.

instance, dry periods are characterized by extensive saline mudflats with efflorescent sodium carbonates and sulfates crusts around a shrunk water body. Furthermore, during extreme low-stands, the lake becomes separated into minor water bodies and typical morphological characteristics of the northeastern part of the Pampean Sand Sea landscape (described by Iriondo and Kröhling, 2007), such as islands, lunettes and dunes, can be observed. Otherwise during the humid phases, the lake expansion floods the mudflats, the salt-crusts are dissolved, and the main water body and wetland areas become the dominant sub-environments (Fig. 1d; Guerra, 2015).

3. Climatic and hydrological setting

3.1. General climate

Climate in the Melincué area is subhumid to humid, the regional average annual precipitation is 980 mm yr^{-1} (1931–2011 period; Fig. 2a and b) and mean annual temperature is 17.5 °C (1940–2013 period; Fig. 2b) (Pasotti et al., 1984; Guerra et al., 2015). The instrumental records show that during the 20th century, water level oscillations in Pampean lakes closely followed the regional rainfall fluctuation (Guerra et al., 2015). Precipitation variability in

Please cite this article in press as: Guerra, L., et al., Climate change evidences from the end of the Little Ice Age to the Current Warm Period registered by Melincué Lake (Northern Pampas, Argentina), Quaternary International (2016), http://dx.doi.org/10.1016/j.quaint.2016.06.033

the eastern Pampas is controlled by low and high frequency changes of the South American Monsoon activity (Zhou and Lau, 1998, 2001; Vera et al., 2006; Garreaud et al., 2009; Fig. 2a). In this atmospheric system, moisture is carried from the Amazonian basin and the Atlantic Ocean to the subtropics of South America through low-level jet streams (South American Low Level Jets, SALLJ), which are in turn regulated by the South Atlantic Convergence Zone (SACZ, Nogués-Paegle and Mo, 2002) and the Atlantic Anticyclone. The SACZ is a convective band with a NW–SE position crossing the continent, reaching the Brazilian coast at 20°S (Carvalho et al., 2004), and whose position and strength depend on the Atlantic sea surface temperature (Doyle and Barros, 2002). Intense SACZ activity is linked to weakened SALLJ, and thus to a diminished moisture transport to Southeastern South America (SESA); whereas a weakened SACZ is associated with an increased southward moisture flux to the subtropical plains (Díaz and Aceituno, 2003; Carvalho et al., 2004).

The activity of the SAM is characterized by a seasonal variation of rainfall, which is controlled by the SALLJ activity, with maximum values during the austral summer (December–March) and minimum during the winter (June–September) (Fig. 2b). Longer-term fluctuations of precipitation in the subtropics of eastern South America can be ascribed to the superposition of large scale ocean-atmosphere features with different frequencies (Garreaud and Aceituno, 2007; Garreaud et al., 2009). On interannual timescales, the El Niño-Southern Oscillation (ENSO) in the tropical Pacific Ocean has been linked to hydrological changes in SESA (Vera et al., 2006). Decadal and multidecadal changes have been connected to atmospheric-ocean coupled oscillations over the Atlantic and the Pacific oceans (Garreaud et al., 2009).

3.2. Documentary and instrumental archives of recent hydroclimate changes

Instrumental and historical lake-level data is available from the beginning of the 20th century (Pasotti et al., 1984; Biasatti et al., 1999; Peralta et al., 2001; Guerra et al., 2015) (Fig. 3a). The annual regional standardized precipitation index (RPI) for the period 1900–2009 (Guerra et al., 2015) was estimated based on precipitation-anomalies of 12 meteorological stations with distances up to 200 km from Melincué Lake. RPI values were calculated according to Jones and Hulme (1996), and Aravena and Luckman (2009). Following the RPI variation pattern between AD 1913 and 2011 the lake level oscillated from 81.00 to 86.13 m a.s.l. (Fig. 3a; Guerra et al., 2015).

In accordance with the maximum instrumentally recorded water level (86.13 m a.s.l. in 2003) and the altitude of the lake-bottom (78.5 m a.s.l., measured in 2011), we proposed to describe the relative water level-stands as quartiles: a) very low to ephemeral (L0 = 78.5–80.4 m); b) low (L1 = 80.4–82.3 m); c) intermediate (L2 = 82.3–84.2 m); and d) high (L3 = 84.2–86.13 m) (Fig. 3a).

For the period prior to the 20th century, historical chronicles and documents suggest the development of extremely arid phases interrupted by short-lived wet events across the Pampean Plains (Cioccale, 1999; Deschamps and Tonni, 2007; Iriondo and Kröhling, 2007; Piovano et al., 2009; Prieto and García Herrera, 2009; Deschamps et al., 2013). Within this climatic context, there are historical chronicles particularly mentioning and describing Melincué Lake conditions. For instance, by AD 1772 historical chronicles described Melincué as a very shallow, swampy and

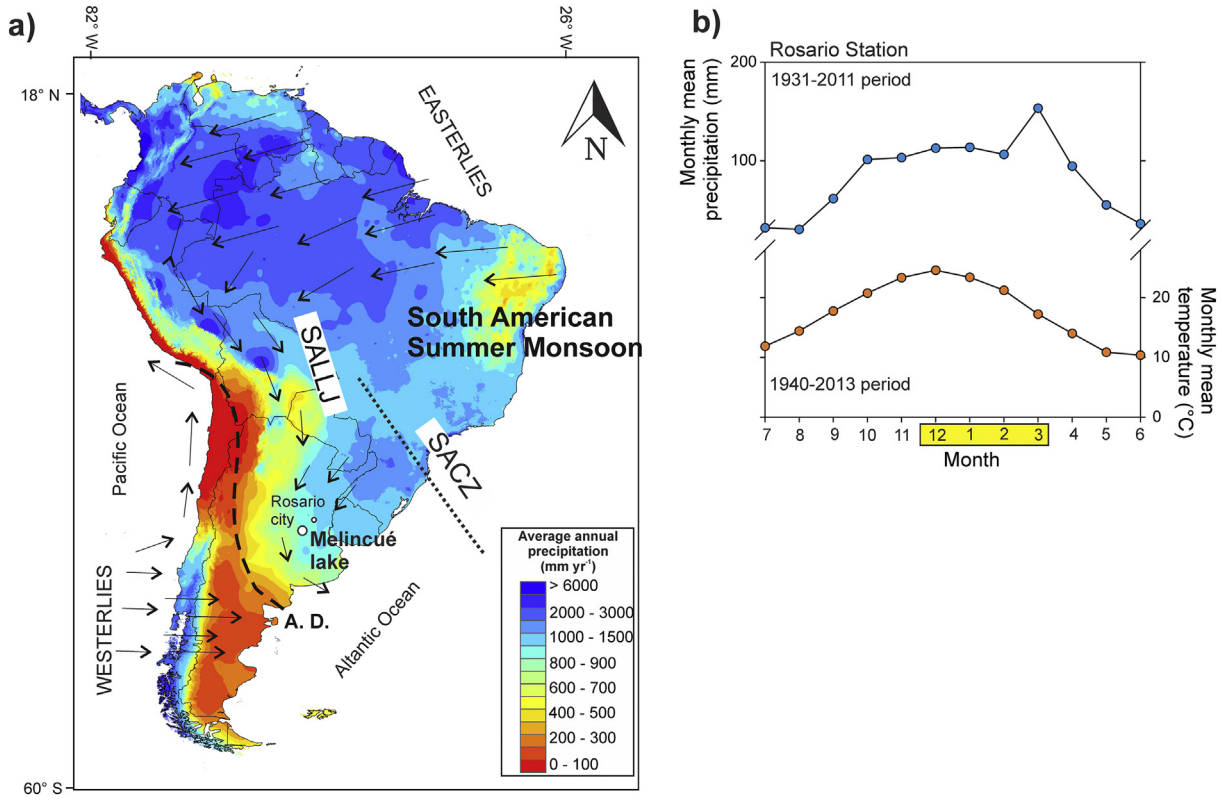

Fig. 2. Climatic setting of the study area. **a)** Mean annual precipitation of South America (modified from Hijmans et al., 2005) showing the main climatic features of South America Monsoon system and the position of the Melincué lake (large white circle). The arrows indicate the direction of the prevailing winds (easterlies and westerlies), and the direction of the South American Low Level Jet (SALLJ) streams. The short-dashed line indicates the position of the South Atlantic Convergence Zone (SACZ) and the long-dashed line shows the Arid Diagonal (Bruniard, 1982), which limits the influence of the SAM (A.D.). **b)** Mean monthly temperature and precipitation for the meteorological station of Rosario (located 150 km distant from Melincué, see location in Fig. 1). Highlighted months indicate the rainy season.

Please cite this article in press as: Guerra, L., et al., Climate change evidences from the end of the Little Ice Age to the Current Warm Period registered by Melincué Lake (Northern Pampas, Argentina), Quaternary International (2016), http://dx.doi.org/10.1016/j.quaint.2016.06.033

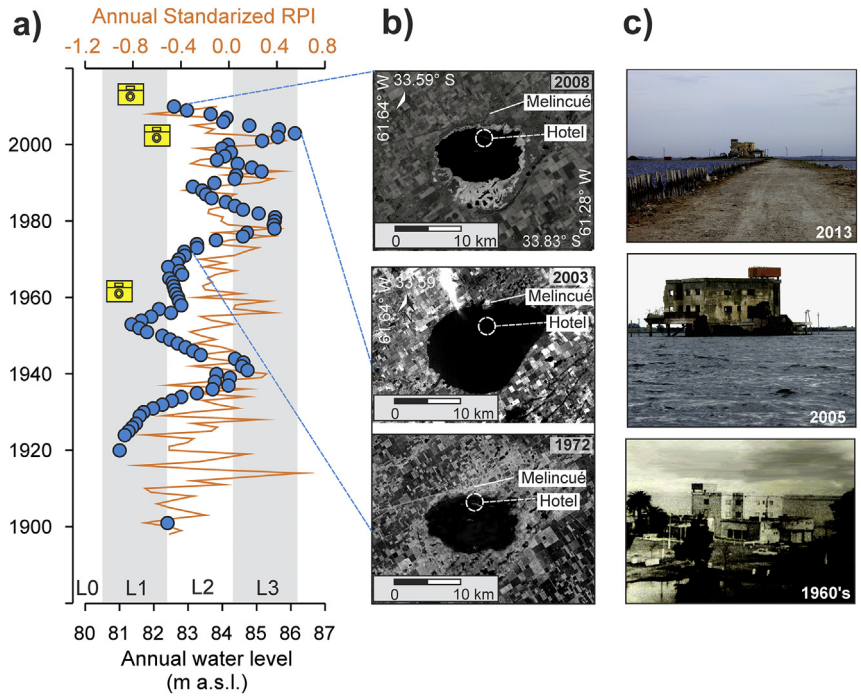

Fig. 3. Hydrological variability during the 20th century. **a)** Annual Regional Precipitation Index (RPI) and annual water level record (m a.s.l.) (Guerra et al., 2015). The boxes indicate the year of the pictures described in c. The shadows indicate the relative lake conditions in four categories: L0 (very shallow to ephemeral); L1 (shallow lake); L2 (intermediate lake); L3 (deep lake). **b)** Landsat (NASA) satellite images of Melincué Lake during lowstand events in 1972 and 2008, and a highstand event in 2003. The circle marks the position of a hotel built during the 20s and 30s on an island flooded during higher lake levels. **c)** Photographs of the hotel during lowstand (1960 and 2013) and the highstand (2005) events.

ephemeral lake with high salinity conditions (Pavón, 1969), likely corresponding to very low-stands (L0).

Later by AD 1796, a detailed travel chronicle described the development of disconnected smaller water bodies, fringed by 4–5 km of evaporitic mudflat, pointing to an extremely shallow lake condition (L0, Azara, 1837). In July AD 1806 a Chilean expeditionary (Luis de la Cruz) estimated the lake perimeter around 16 km ("~3 leagues", corresponding to a shoreline at ~80.8 m a.s.l., L0-L1), and presumed former lake-level oscillations (Gatti, 2010). Historical documents also indicate that during the following year, (i.e. AD, 1807), the lake circumference was ~32 km, corresponding to a shoreline at ~82.5 m a.s.l. (L1), alike the limnimetric record of AD 2009 (Gatti, 2010). From AD 1827 to AD 1832, an extended aridity phase in central Argentina was documented by Darwin (1860) and named as the "Great Drought". Darwin described that during this dry stage the vegetation failed, many animals perished and the small rivers became saline as a consequence of aridity. During this phase, most of the Pampean lakes were dried-out, allowing for the inference of very low water levels in Melincué Lake (L0) in agreement with the regional tendency. In the next years, Darwin documented a rainy season with important floods for the same region and probably Melincué lake-level followed the regional pattern (L1). By the end of the 19th century, a major flood of the Paraná River in AD 1877–1878 linked to a strong El-Niño was reported in Rosario city, located 150 km northeast from Melincué (Aceituno et al., 2009; Fig. 1a and b). This hydrological event matched with high precipitation records in Córdoba and Santa Fe, water-level increases of lake-levels and river discharges from La Plata basin (Aceituno et al., 2009). The areal magnitude of the event likely triggered a level increase at Melincué Lake (L3) for that time.

Along the 20th century the lake-water levels started to be monitored, as their oscillations negatively impacted on the socio-economic development of Melincué (Fig. 3c). From the early 20th century until the end of the 1930s, data show dominant negative RPI values matching low lake levels (L1). During this low-stand, a hotel was built on an island located at 1 km from the northern coast of Melincué lake above the 84.35 m a.s.l. altitude (Fig. 3c; L1-L2). This island and other topographic heights emerge during the low-stands when the water levels are below 84 m a.s.l., and become flooded during high-stand periods (Figs. 1d, 3b and c). In the 1940s, the instrumental records show the presence of a humid pulse (L2-L3). Afterwards, a negative lake-level tendency prolonged until the 1970s, when a long period of intense rainfall started in the region. During this intensively humid period a widespread water levels increase was synchronically register across the Pampean lakes (e.g. Troin et al., 2010; Córdoba et al., 2014). including Melincué system (L2-L3).

4. Materials and methods

4.1. Magnetic, sedimentological and geochemical methods

Triplicate short cores (M8A, M8B and M8C; length < 126 cm) from the deepest part of the lake (33°42′50.7″S/61°22′23″W; Fig. 1c) were retrieved in May 2011, using a Beaker-type sediment hand corer (Eijkelkamp), to provide the material for multi-proxy analyses. The cores were cut in two halves and stored at 4 °C. Volumetric Magnetic Susceptibility (MS) was measured using a MS2E Bartington sensor every 0.5 cm on each core half.

Visual descriptions of sedimentary units, depositional structures and discontinuities were further corroborated by inspecting sedimentological and physico-chemical data changes along the sequence.

The mean particle size was determined for samples using a laser diffraction grain size analyzer (HORIBA LA-950). Samples, taken at ca. every 5 cm, were pre-treated with 20 ml of 30% H_2O_2 to eliminate the organic matter, and with 20 ml HCl (10%) to remove the carbonates. Then, this material was rinsed with distilled water and the residue was dispersed with 10 ml of $(NaPO_3)_6$ solution to prevent particles from aggregating.

Please cite this article in press as: Guerra, L., et al., Climate change evidences from the end of the Little Ice Age to the Current Warm Period registered by Melincué Lake (Northern Pampas, Argentina), Quaternary International (2016), http://dx.doi.org/10.1016/j.quaint.2016.06.033

Major mineralogy was identified at ~10 cm interval by X-ray diffraction (XRD). Approximately 1 cm^3 of dried bulk sediment samples were ground in an agate mortar and then sieved through a 63-μm stainless steel mesh. Samples were scanned using an X'Pert PRO-Analytical Diffractometer (Facultad de Ciencias Químicas, Universidad Nacional de Córdoba) with a Cu anode (Cu Kα = 1.5406 Å) and a detection between 5° and ca. 65° 2θ angles. Peak identification and position was determined using Bragg's law and comparing the obtained diffractograms with known mineral patterns. Major and trace elements (Al, Si, Ti, Ca, Sr and K) were measured at 5 mm-resolution using an XRF core scanner (ITRAX, Cox Analytical Systems; Croudace et al., 2006), at the Centre Européen de Recherche et d'Enseignement des Géosciences de l'Environnement (CEREGE) in Aix-en-Provence (France). Measurement conditions were: 15s exposition times, 30 kV X-ray voltage, and X-ray current of 40 mA using a Cr tube as the X-ray source. The X-ray fluorescence technique enabled rapid and non-destructive measurements, providing semi-quantitative and high-resolution elemental data in the lake sedimentary core. Results from the XRF core scanner were expressed as XRF intensities (counts) that are proportional to relative element concentrations.

Total nitrogen (TN), total organic carbon (TOC) and total inorganic carbon data (TIC) were determined by means of flash combustion and gas-chromatography separation, and detected by thermal conductivity using a CNS elemental analyzer at CEREGE (NA Fisons; Guerra et al., 2015). Results were compared with the XRF information. Dry bulk density was estimated as a function of water, inorganic and organic content from sediment samples following Binford (1990).

$$\rho x = [D(2.5Ix + 1.6Cx)/[D + (1 - D)(2.5Ix + 1.6Cx)] \quad (1)$$

In the Equation (1), $\boldsymbol{\rho}$ is the dry material density ($g_{dry}\,cm^{-3}{}_{wet}$), $\boldsymbol{x}$ is the core depth (cm or g cm^{-2}), $\boldsymbol{D}$ is the proportion of dry weight by wet volume, $\boldsymbol{I}$ is the inorganic proportion of dry material (density = 2.5 g cm^{-3}) and $\boldsymbol{C}$ is the organic proportion of the dry material (density = 1.6 g cm^{-3}).

A Principal Component Analysis was performed using R-commander (http://www.r-project.org/) and PAST v2.14 (Hammer et al., 2001) software packages, in order to reduce the variable space and to better understand the different controls on element variability and co-variability in the core. The dataset included the XRF elements (Al, Si, Ti, Ca, Sr, K, Fe) and the MS, as well as TOC, TN, TIC, dry bulk density and TOC/TN (obtained by Guerra et al., 2015).

4.2. Core correlation and chronology

Since the analyses (i.e. CNS measurements, XRF determinations and age models; Fig. 4a) were performed on different cores, the development of an accurate correlation was crucial. Sediment cores were correlated using the CPLSlot software (Thompson et al., 2012) based on magnetic susceptibility variability (Fig. 4b) and constrained with the most noticeable lithological and geochemical features.

The chronology framework, based on ^{210}Pb and ^{14}C dating techniques, was previously developed by Guerra et al. (2015). The age model included ^{210}Pb ages for the 80 cm upper from the M8A master core, considering the Constant Rate of Supply model (CRS, Robbins, 1978; Appleby, 2008), following Sanchez-Cabeza and Ruiz-Fernández (2012) for calculation and Binford (1990) for dry bulk density estimations (Fig. 4a). A chronological marker (AD, 1976 ± 4) corresponding to an organic-rich level, which is the record of a regional well-registered hydroclimatic wet pulse (e.g. Piovano et al., 2002; Coianiz et al., 2015; Córdoba et al., in this volume; Guerra et al., 2015), was used to constrain the derived ^{210}Pb ages.

In order to convert all core depths into ages, cubic splines were applied on each correlated core (e.g. Thompson et al., 2012) through the equation:

$$Age = y_0 + ax + bx^2 + cx^3 \quad (2)$$

In this equation, $\boldsymbol{x}$ represents the CRS-dated sample-depth (in cm), $\boldsymbol{y_0}$ corresponds to the date when the core was retrieved (i.e. 2011.25), and $\boldsymbol{a}$, $\boldsymbol{b}$ and $\boldsymbol{c}$ are coefficients for each spline (Table 1, Fig. 4c).

Table 1
Spline estimates and coefficients.

	M8A	M8B	M8C
y_0	2011.25	2011.25	2011.25
a	−1.3675	−1.6738	−2.0867
b	0.0104	0.0167	0.0193
c	−0.0002	−0.0003	−0.0003
r^a	0.9994	0.9995	0.9953
SE	1.6894	2.24	5.31

SE = standard error.
[a] r = Pearson correlation coefficients.

A radiocarbon age of AD 1492 ± 59 (median of the 2σ probability = 324–513 cal BP) was determined in an organic-rich interval (90.5–91.5 cm) from M8B core (Fig. 4a). It was calibrated using the Calib 7.0 software package (Stuiver and Reimer, 1993) and modeled with the SHCal13 curve (Hogg et al., 2013), selecting medians of the 95.4% distribution (Fig. 4a).

4.3. Regional analysis

The environmental changes occurring from the end of the LIA to the CWP were evaluated on a large-spatial perspective by comparing the Melincué hydroclimatic reconstruction with other paleoclimatic records. We first analyzed the link between our geochemical data, the regional precipitation index (the RPI; and the 5-year moving average) and the Melincué Lake annual water-level variation (Guerra et al., 2015). The water level oscillations of Mar Chiquita Lake (Piovano et al., 2002) were also considered to explore the regional pattern of precipitation-evaporation balance changes.

In order to identify the changes of precipitation in Melincué region associated to the SAM source of moisture (i.e. the Atlantic Ocean), we compared the Melincué records with the sea surface temperature anomaly (SST, °C) reconstruction from the Tropical Western Atlantic obtained by Tierney et al. (2015). Considering that the SAM is additionally influenced by other climatic modes, such as ENSO (see Section 3.1), we also included in the analyses the El Niño 3.4 index (i.e. in the Central Equatorial Pacific region) reconstructed by Li et al. (2013). Both SST and El Niño 3.4 index were obtained from the National Oceanic and Atmospheric Administration (NOAA database).

5. Results

5.1. Stratigraphy and sediment composition

Age-depth profiles showing the analyzed sedimentary, physical and geochemical proxies are displayed in Fig. 5. In order to make descriptions consistent, depths and ages correspond to the M8B spline (Fig. 4c). Sedimentary features allowed the identification of contrasting records that can be divided into three sedimentary units: UC, UB and UA.

Unit C is composed of massive sediments from the lowermost 17 cm between the base of the core and the ~73 cm level. These sediments accumulated between AD 1492 and AD 1880 ± 20,

Please cite this article in press as: Guerra, L., et al., Climate change evidences from the end of the Little Ice Age to the Current Warm Period registered by Melincué Lake (Northern Pampas, Argentina), Quaternary International (2016), http://dx.doi.org/10.1016/j.quaint.2016.06.033

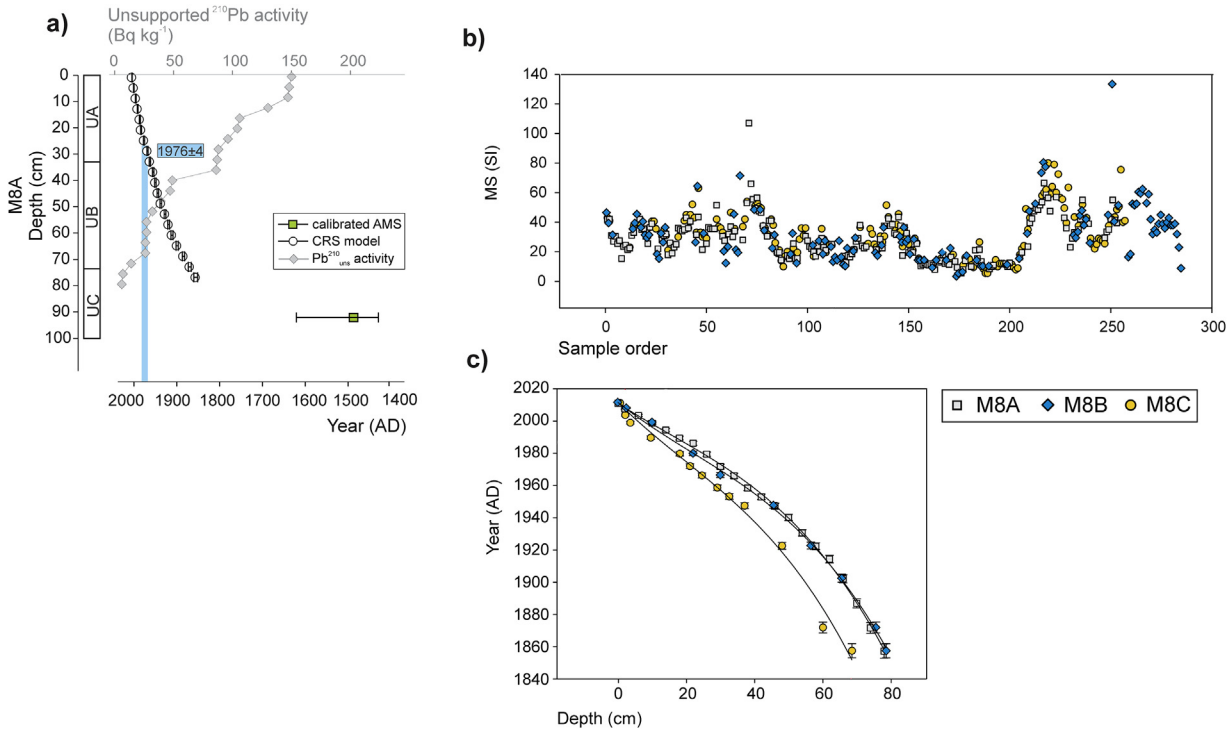

Fig. 4. Chronological model, slotting and correlation of sedimentary cores M8A, M8B and M8C. **a)** ^{210}Pb unsupported activity (diamonds) and CRS modeled ages (circles) from the M8A dated master core, and AMS calibrated age (year AD), modified from Guerra et al. (2015). The vertical bar corresponds to the 1976 ± 4 chronostratigraphic control age. **b)** Magnetic susceptibility of cores M8A, M8B and M8C, used for core correlation and sequence slotting. **c)** Time-depth profile of the 3rd order polynomial derived curves based on the modeled CRS ages (M8A core) vs. the core depths in M8A, M8B and M8C.

indicating a minimum sedimentation rate value of ~0.04 cm yr^{-1}for this unit. It is formed by grey medium to coarse silty facies (mean particle size = 19–39 μm), with high magnetic susceptibility and low organic matter percentages, (i.e. TOC and TN < 0.15 and 0.05%, respectively; Fig. 5). TOC/TN ratio values > 20 allow considering a terrestrial organic matter source (Meyers, 1994). Si, Ti, K, Fe, Ca, Al and Sr are in high proportions in this unit.

The top of the UC presents a sharp limit marked by an abrupt physical and geochemical shift. Over this contact, massive silts from UC turn into organic-rich (TOC and TN > 0.15 and 0.05%, respectively), bedded and laminated silty facies, forming units UB and UA (from 73 cm in M8B core up to the surface) (Fig. 5). This section accumulated between AD 1880 ± 20 and the present, yielding a minimum sedimentation rate of 0.5 cm yr^{-1}. Dry bulk density also shows contrasting values between both core sections, ranging from 0.7 gcm^{-3} in the lowermost 20 cm of the core to 0.4 gcm^{-3} in the 73 cm upper section. The TOC/TN ratio is significantly reduced to values < 15 above the contact.

The base of UB is characterized by decreasing values of MS and low Ca, Fe and Sr counts upwards the unit. Similarly, K, Al, Ti and Si counts show low values at the base of UB, followed by an increase between 55 and ~45 cm depths (ca. AD, 1915–1920). The mean particle size oscillates between 13 and 42 μm, with a noticeable coarsening at 47 cm level (ca.AD, 1940).

At ~30 cm depth (AD, 1972 ± 2) there is a gradational contact overlying UA. UA is characterized by ochre and dark brown, laminated, organic-rich fine and medium silts (medium grain size from 15 to 26 μm). Upwards this unit Ti, Al, Si and K counts as well as organic matter contents (TOC and TN) rise simultaneously. In contrast, Ca, Sr, Fe and TIC show a marked concomitant decrease at the base of UA. Above 10 cm level (ca. AD, 1983), the Ti, Al, Si and K intensities show an increase trend towards the top of the core.

The major mineral components of all units include quartz [SiO_2] + muscovite/illite [$KAl_2(AlSi_3)O_{10}(OH)_2$/$(K,H_3O)(Al,Mg,Fe)_2(Si,Al)_4O_{10}[(OH)_2,(H_2O)]$] + plagioclases [$(Na,Ca)(Si,Al)_4O_8$] + calcite [$CaCO_3$] + bloedite [$Na_2Mg(SO_4)_2{\cdot}4(H_2O)$] (Fig. 6). In discrete samples, nahcolite [$NaCO_3$], cordierite [$(Mg,Fe)_2Al_4Si_5O_{18}$], despujolsite [$Ca_3Mn(SO_4)_2(OH)_6{\cdot}3(H_2O)$], anhydrite [$CaSO_4$], titanite [$CaTiSiO_5$], clinoptilolite [$(Ca,K,Na)_6(Si_{30}Al_6)O_{72}{\cdot}20H_2O$], nontronite [$Na_{0.3}Fe^{3+}_2Si_3AlO_{10}(OH)_2{\cdot}4(H_2O)$], gypsum [$CaSO_4{\cdot}2H_2O$] and thermonatrite [$Na_2CO_3{\cdot}H_2O$] were also detected (Table 2).

Table 2
Mineralogy for sedimentary M8B core samples.

Core-sample	Depth (cm)	Unit	Mineralogy
M8B-123	0.75	A	quartz-plagioclase-muscovite/illite-calcite
M8B-112	11.75	A	quartz-muscovite/illite-despujolsite-calcite-cordierite-plagioclase
M8B-103	20.75	A	quartz-muscovite/illite-bloedite-calcite-nahcolite-plagioclase
M8B-91	32	A	quartz-plagioclase-muscovite/illite-calcite-bloedite-
M8B-82	42	B	quartz-plagioclase-muscovite/illite-bloedite-calcite-nahcolite-anhydrite-titanite
M8B-71	53	B	quartz-bloedite-clinoptilolite-gypsum-thermonatrite-plagioclase-calcite
M8B-61	63	B	quartz-plagioclase-calcite-muscovite/illite-nontronite-nahcolite-titanite
M8B-50	74	B	quartz-plagioclase-calcite-illite-bloedite
M8B-45	79	C	quartz-plagioclase-calcite-muscovite/illite-bloedite
M8B-34	90	C	quartz-calcite-plagioclase-bloedite-muscovite/illite-nahcolite

5.2. Principal Component Analysis

A PCA for a dataset of 13 standardized variables (Ti, Al, Si, Ca, K, Sr, Fe, MS, TOC, TIC, TN, TOC/TN and dry bulk density), was applied

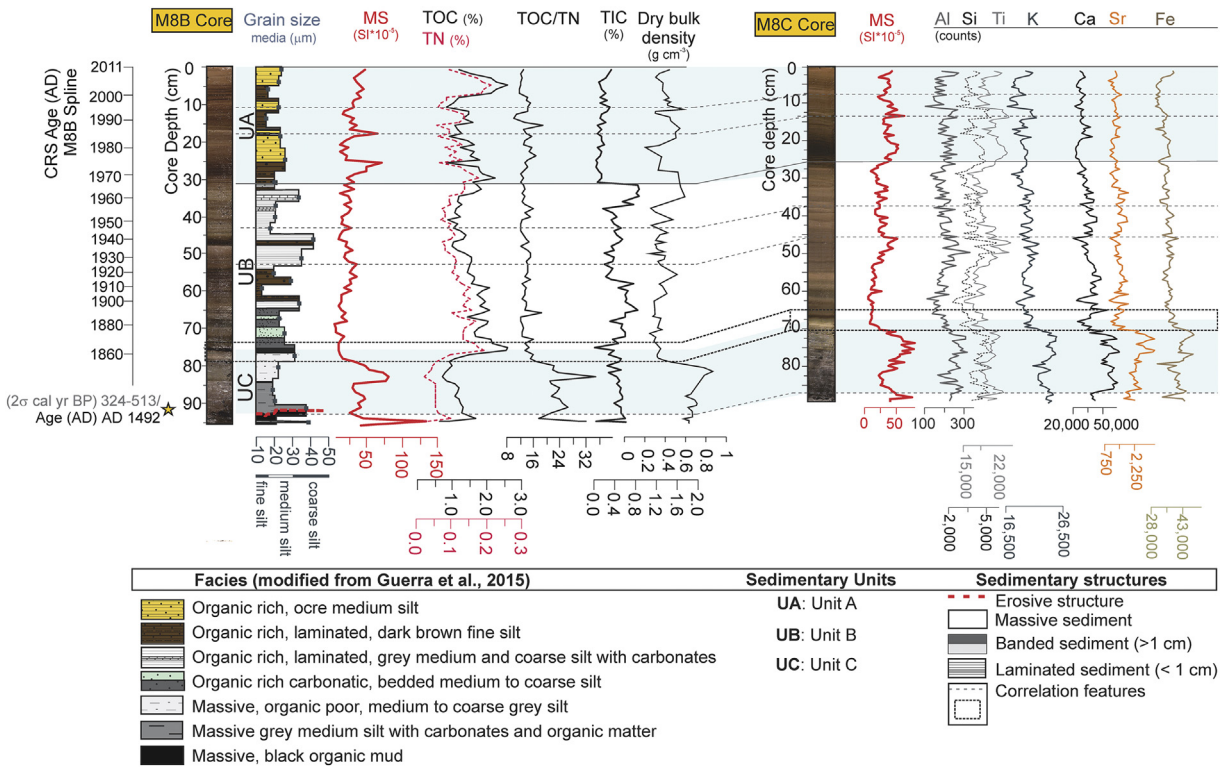

Fig. 5. Stratigraphy and geochemistry of the cores. From left to right: CRS modeled ages (from M8B spline; Fig. 4, Table 1) and the calibrated radiocarbon age; sedimentary facies and units, magnetic susceptibility (MS, expressed as standard units in the M8B core), total organic carbon (TOC), nitrogen (TN) and inorganic carbon (TIC), expressed as percentages in M8B core; TOC/TN ratio and dry bulk density (g cm^{-3}); photograph, magnetic susceptibility (MS; M8C core) and elemental variation (expressed as XRF counts). Some correlation features are highlighted as dashed lines.

in order to understand the dependence among variables and discriminate the underlying processes controlling sediment deposition. Since the variables were measured with different sampling resolution (~1 cm in M8B core, and 0.5 cm in M8A), correlation and minimum resolution was preferred for calculation.

Two eigenvectors (PC1 and PC2) accounted for 78.74% of the variance. The PC 1 explained the 50.89% of the total variance showing a positive correlation with all the XRF elements and with the TOC/TN ratio, the dry bulk density and the MS. In contrast, negative correlation with TOC and TN was observed (Fig. 7, Table 3).

Table 3
Principal component analysis. Factor loadings for the variables in the two principal components (PC 1 and PC 2).

Loading coefficients	PC 1	PC 2
Al	0.717	0.191
Si	0.6924	0.537
Ca	0.7162	−0.5039
Ti	0.4249	0.8286
K	0.928	−0.0781
Fe	0.6546	−0.1334
Sr	0.8706	−0.353
MS	0.6854	0.4735
TN	−0.7752	0.1935
TOC/TN	0.8638	−0.2113
TOC	−0.6158	0.1442
TIC	0.0288	−0.7328
Dry bulk density	0.8274	0.103

The PC 2 represented the 17.61% of the total variance, and it was mostly controlled by Ti and Si at the positive end, and by TIC and Ca at the negative end (Fig. 7, Table 3).

6. Discussion

6.1. Environmental significance of the variables and hydroclimate implications

Factor loadings in the PCA analysis (Table 3) highlight that PC 1 is defined by two groups of variables: a) K, dry bulk density, Sr, Ca and TOC/TN, in contraposition with b) TOC and TN (Fig. 7).

Elements such as K, Al, Si and Ti are associated to aluminosilicate minerals composing sediments (e.g. Boës et al., 2011; Burnett et al., 2011). Plagioclases, quartz, micas and clays were detected in all analyzed sediment samples and they are abundant components of the Pampean loess surrounding the lake area (Kröhling, 1999; Kröhling and Orfeo, 2002). Additionally, a close relationship between Fe and Al counts (Fig. 8a) points to consider the terrigenous influx as an important control of iron.

Fig. 5 shows that the MS curve diverges from the Fe counts variation (i.e. more Fe concentration is not reflected as a MS increases), whereas it is more closely linked to the dry bulk density changes. Magnetic susceptibility values, which are mainly controlled by the concentration and composition of ferrimagnetic mineral, can be affected by dilution effects showing low values in organic matter-rich sediments (Dearing, 1994). Consistently, while marked lower densities characterize organic-rich sediments increased values characterize the organic-poor ones. The opposed relationship between physical proxies and the TN (and TOC) percentages emphasizes a role of PC 1 as tracer of clastic fluxes vs. organic matter accumulation changes.

The positive correlation of TOC/TN ratio with PC 1 observed in Table 3 can be explained by the variation of the lake primary productivity. While increased TOC/TN ratios in the sediments characterize low primary productivity and predominant detrital organic

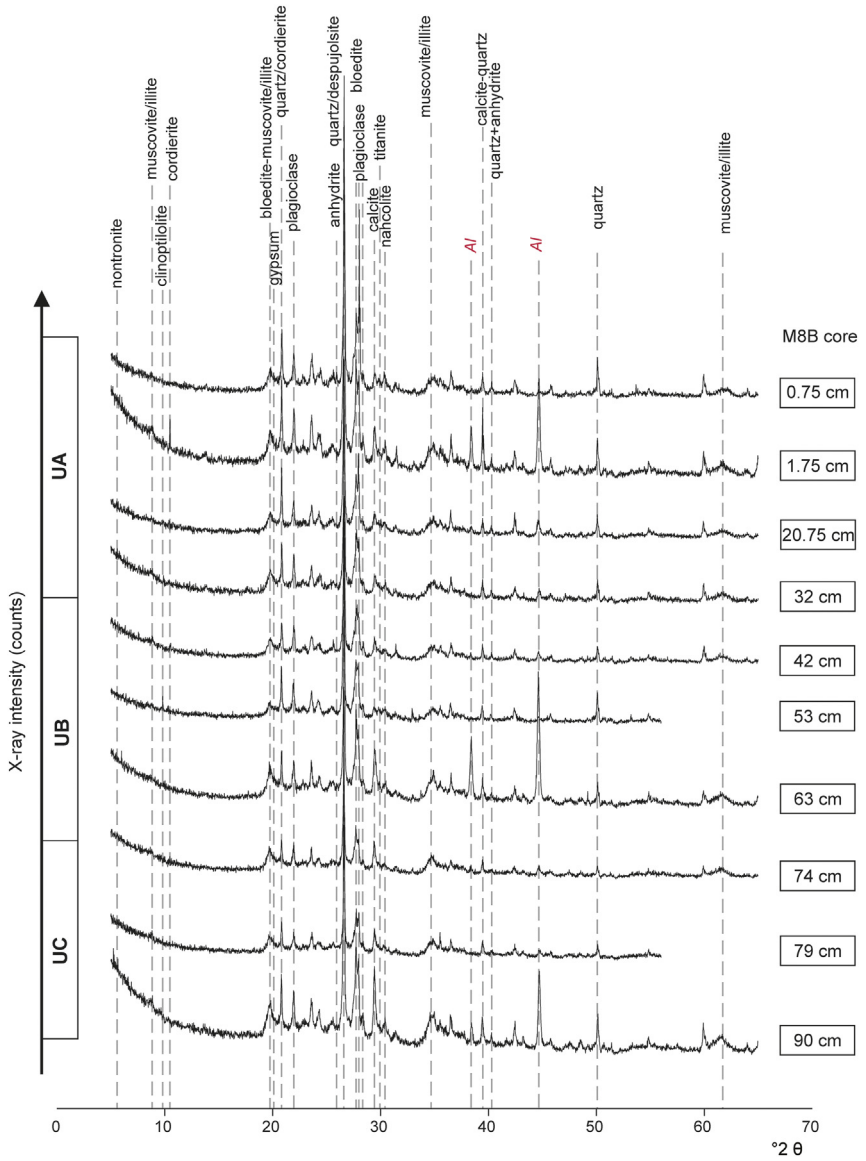

Fig. 6. X-ray diffractograms (2θ vs. X-ray intensity) and identified minerals of the lacustrine sediment samples. Only some of the diagnostic mineral peaks are detailed on the labels. Sedimentary units (UA, UB and UC) and sample depths indicated in boxes correspond to the M8B core. Peaks identified as Al correspond to the aluminum sample holder.

matter sources, low ratios evidence autochthonous organic matter (Meyers, 1994; 2003). The sedimentary record of different shallow Pampean lakes shows that increased TOC and TN are linked to an enhanced productivity at high-lake levels. Melincué Lake expansions during wet phases invoke a positive feedback mechanism between the development of larger littoral areas promoting phytoplankton growth (Romano et al., 2005) and increasing the autochthonous organic matter preserved in the lake sediments.

The second eigenvector (PC 2) is mainly associated with Ti in the positive end, and with TIC and Ca in the negative end. The ratio of Ca intensity against a conservative element such as Ti or Al allows discriminating the signal of within-lake precipitation from the allogenic material. In Fig. 8c, the Ca/Ti ratio is positively correlated with the TIC percentages. High TIC contents and Ca/Ti values are typically associated to evaporitic, endogenic or biogenic carbonates, and their presence in closed lake sediments evidences high alkalinity and salinity conditions (e.g. Burnett et al., 2011; Martín-Puertas et al., 2011). Carbonate minerals (e.g., calcite, nahcolite), along with sulfates (e.g. bloedite, and occasionally anhydrite, gypsum) in the core sediments (Fig. 6; Table 2), can be formed within the lake or as evaporitic crusts under negative precipitation-evaporation balances (e.g. Last and Ginn, 2005; Haberzettl et al., 2007; Warren, 2010; Brown, 2011; Zanor et al., 2012), as occurred in the current-day mudflats of Melincué by evaporative pumping (Guerra et al., 2015, Fig. 1d). Additionally, biogenically-produced carbonate can also be found in form of i.e. ostracod shells in the laminated muds from the Units A and B. Therefore, the PC 2 can be related to authigenic or endogenic precipitation of carbonates under negative water balances in dry hydroclimate conditions.

PCA results show that different processes combined and prevailed during the units' formation (Table 4). The sample distribution on the PCA indicates that massive organic-poor silts from UC are associated with positive PC 1 and thus, ruled by clastic fluxes along with low organic matter accumulation from a predominantly terrestrial origin. These conditions concurred with important endogenic/authigenic mineral precipitation (negative PC 2). The combination of the variables indicates that the interpreted processes have occurred in a very shallow environment that prevented the autochthonous organic matter growth and preservation. The lack of lamination structures and low sedimentation

Please cite this article in press as: Guerra, L., et al., Climate change evidences from the end of the Little Ice Age to the Current Warm Period registered by Melincué Lake (Northern Pampas, Argentina), Quaternary International (2016), http://dx.doi.org/10.1016/j.quaint.2016.06.033

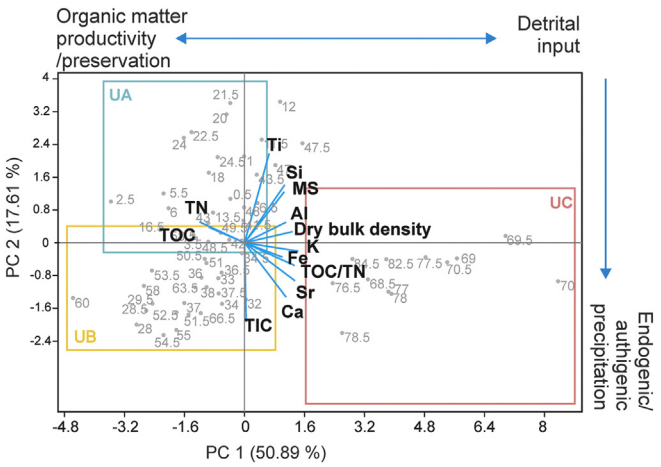

Fig. 7. Principal Component Analysis biplot (PC 1 vs PC 2) and distribution of the samples. Dataset analyses 13 variables, including Ti, Si, Al, Ca, Sr, K, Fe, magnetic susceptibility (MS), total organic and inorganic carbon (TOC and TIC), total nitrogen (TN), TOC/TN ratio and dry bulk density. PC 1 highlights the detrital allogenic input vs. the organic matter accumulation; and PC 2 reflects authigenic/endogenic precipitation processes. The square areas enclose the samples according to the sedimentary unit (UA, UB or UC). The ellipses show three main variable groups.

rates support the interpretation and evidence ephemeral conditions.

UB sediment samples associated with negative PC 1 marks an environmental change reflected by enhanced primary productivity and organic matter accumulation causing the dilution of the detrital elements (Fig. 7). This environmental change from UC to UB sediments is also presented in the K vs. TOC plot (Fig. 8b). These results, along with lamination preservation, allow us to infer the settlement of perennial conditions. Nevertheless, the distribution of samples respecting to PC 2 reveals dominant endogenic/authigenic mineral precipitation (Fig. 7). In addition, variable particle sizes (Fig. 5) indicate alternation of profundal subenvironments during intermedium to high lake-levels (L1-L2) and lake retraction stages with the development of littoral nearshore environments (L1).

The fine organic-rich sediments from Unit UA show variable distribution respecting to PC 1, which represent a combination of high detrital delivery to the lake-bottom and important primary organic-matter accumulation. Although the detrital elements increase in this unit, indicating increased detrital influxes, lower salinities (i.e. positive PC 2, Fig. 7) and fine grain sizes (Fig. 5) evidence the development of distal and more profundal environments (lake-level L2-L3) and subsaline water conditions. A synthesis of the environmental interpretations and the lake-levels interpreted for each unit is presented in Table 4.

Table 4
Environmental interpretation of the sedimentary units.

Unit	Year (AD) [M8B spline]	Geochemical and magnetic properties (relative proportions)	Paleo-lake level	Environmental interpretation
A	~1972–2011	High Ti, Si, Al (at the base of the unit) Low Fe High MS, low bulk density Low TIC, Cal and Sr High TOC and TN Low TOC/TN Medium to fine silts	L2-L3	Perennial, subsaline lake. High productivity and organic matter preservation. Predominant water-runoff detrital influx of fine particles
B	~1880–1972	Variable Si, Fe, K, Ti and Al Low MS and bulk density Low Ca and Sr, high TIC High TOC and TN Low TOC/TN Predominant medium and coarse silts	L1-L2-L3	Perennial, saline to subsaline lake. Endogenic/authigenic carbonates precipitation. High primary productivity. Variable detrital influx.
C	~1492–1880	High Ti, Si and Al High K and Fe High MS and bulk density High Ca Sr and TIC Low TOC and TN High TOC/TN Medium to coarse silts	L0-L1	Saline very shallow and ephemeral to shallow lake. Low primary productivity and organic matter preservation. Preferential detritial accumulation.

Sedimentary units (UA, UB, UC), properties, interpreted paleolake-levels (L0, L1, L2, L3, see the text for further explanations) and paleoenvironmental interpretation.

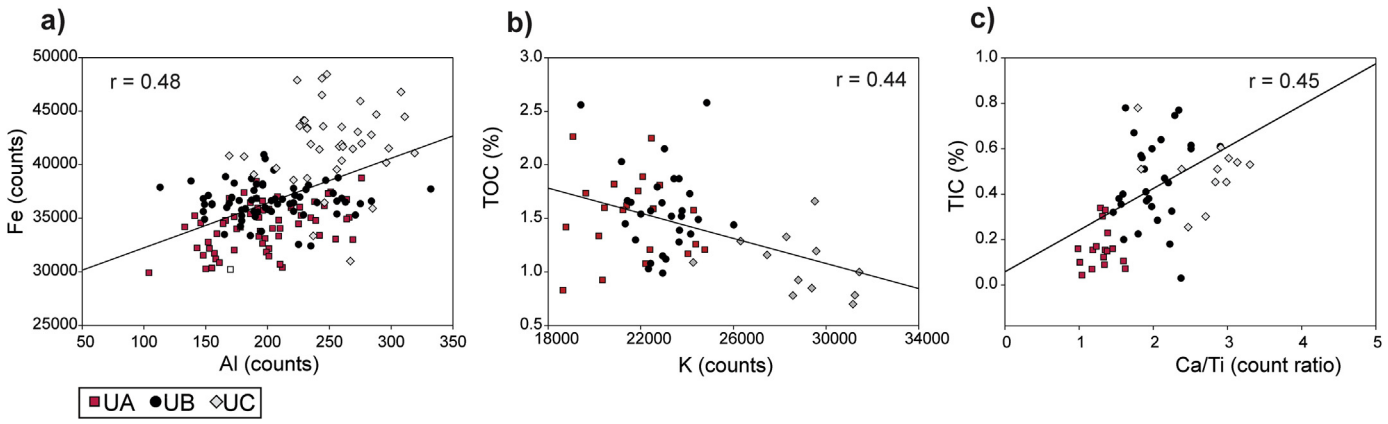

Fig. 8. Elemental ratios and linear regression of samples according to the sedimentary units: UA (squares), UB (dark dots), UC (diamonds). **a)** Fe vs. Al (XRF counts). **b)** Total organic carbon (TOC %) vs. K (XRF counts). **c)** Total inorganic carbon vs. Ca/Ti ratio.

Please cite this article in press as: Guerra, L., et al., Climate change evidences from the end of the Little Ice Age to the Current Warm Period registered by Melincué Lake (Northern Pampas, Argentina), Quaternary International (2016), http://dx.doi.org/10.1016/j.quaint.2016.06.033

6.2. Hydrological reconstruction: records of LIA and CWP in Melincué Lake and South America

An integration of geochemical data (synthesized by PC 1 and PC 2), instrumental record (lake-water level and RPI) and historical information covering the end of the LIA and the CWP is presented in Fig. 9a–d. Very low sedimentation rates during deposition of UC suggest the presence of sedimentary hiatuses, which precluded extending ^{210}Pb ages prior to AD 1860. Consequently, a continuous chronological model could not be applied along the LIA sedimentary record. The analyzed records are compared with other South American records and paleoclimatic indicators such as the Mar Chiquita Lake level variations (30°S–62°W; Piovano et al., 2002; Fig. 9e), SST anomalies in the Atlantic (Tierney et al., 2015; Fig. 9f) and Pacific Oceans (Li et al., 2013, Fig. 9g) to further evaluate the incidence of climatic forcings on hydrological changes in the Pampean plains.

6.2.1. Climate by the end of the Little Ice Age and hydroclimate changes during Current Warm Period an enter is missing

Numerous global paleoceanographic models demonstrate cooling trends in the sea surface temperature from AD 1500–1580 until AD 1800–1880 (PAGES 2k Consortium, 2013; McGregor et al., 2015). Particularly, the temperature-anomalies reconstructed on the western Atlantic by Tierney et al. (2015) show cooling conditions until the 1830s and distinguish the coolest decade from AD 1825 to AD 1834 (−0.7 °C), during the last part of the LIA (Fig. 9f). Cold phases with frequent extreme droughts and floods were also defined for the Argentinean Pampas and Uruguay coincidently with the LIA (Cioccale, 1999; Piovano et al., 2002; Deschamps and Tonni, 2007; Iriondo and Kröhling, 2007; Prieto and García Herrera, 2009; García-Rodríguez et al., 2009; Laprida et al., 2009; Laprida and Valero-Garcés, 2009; del Puerto et al., 2013; Córdoba et al., 2014; Coianiz et al., 2015), supporting a general consistency on the timing across southeastern South America.

Historical records from Melincué Lake, previous to the 20th century, indicate the very low lake-levels (L0-L1) and the development of broad evaporitic mudflats fringing the lake, coincident with the LIA (Fig. 9d). Geochemical proxies of UC indicate a dominant allochthonous lithogenic input (Fig. 9a) during a very shallow and ephemeral water stage by the 19th century, and high salinity and alkalinity, as pointed by low PC 2 (Fig. 9b). Therefore, the analyzed geochemical data and the dominance of massive sediments in UC (Fig. 5) provide reliable evidences to infer lacustrine retractions at dominant drought scenarios during the end of the LIA period. In agreement, the last part of the LIA, shown in Fig. 9f and g, matches reduced anomalies in El Niño SST reconstruction and dominantly negative SST anomalies in the Atlantic Ocean record (Fig. 9f and g).

Several South American paleoclimatological records have identified a general temperature increase after the LIA in the eastern tropical Andes (e.g. Bird et al., 2011; Vuille et al., 2012; Thompson et al., 2013) and along southeastern South America (e.g. Córdoba et al., 2014; Laprida et al., 2014b). In Melincué Lake the paleolimnological record showed an abrupt increase of the sedimentary rates, a shift in the organic matter source as well as in the geochemical fingerprint of sediments from UC to UB (Fig. 5), which can be ascribed to the onset of a perennial lake setting by the end of 19th century. UB, composed of banded and laminated silts with well-preserved mixed (terrestrial and lacustrine) organic matter, allowed to consider permanent lake conditions and thus a wetter setting during this time (Fig. 9a and b). On a regional scale, shifts from ephemeral and playa-lake systems to permanent lakes were recognized in different climate archives from northern (Mar Chiquita lake; 30°S–62°W) to southwestern Pampean Plains (Lagunas Encadenadas del Oeste system; 37°S–62°O; Córdoba et al., 2014) pointing towards a regional hydrological change (Piovano et al., 2014). The timing of this wet pulse coincides with the important rainfall and river runoff increases, which occurred in southeastern South America by AD 1877–1878, attributed to an important El Niño phase (Aceituno et al., 2009; Fig. 9d). In addition, the records of SST of the tropical Western Atlantic (Tierney et al., 2015) and Equatorial Pacific oceans (Li et al., 2013) show strong positive pulses centered at AD 1870–1890 (Fig. 9f and g). The synchronic response of multiple proxy data suggest an important hydroclimatic change -manifested as a widespread precipitation increase in the Argentinean Pampas-occurring after ~ AD 1878 that is consistent with the beginning of the CWP in South America (Bird et al., 2011; Vuille et al., 2012; Thompson et al., 2013).

Following the lake expansion by the end of the 19th century, several indicators allow the inference of low-stands until the 1930s (L1; Fig. 9d), accompanied by saline water conditions (i.e. pointed by negative PC 2increases; Fig. 9b). Afterwards, the historical and instrumental data, allowed for the identification of wetter conditions (i.e. positive RPIs and intermediate to high lake levels; L2-L3) lasting from the end of 1930s decade until the beginning of 1960s. During this wetter stage, sustained freshwater supply can be considered due to a progressive rainfall rise in the area (see RPI values in Fig. 9d).

After the beginning of the 1960s, water level drops can be identified in the instrumental record of Melincué Lake and other Pampean lakes such as Mar Chiquita (Piovano et al., 2009; Fig. 9c and e). The widespread lake areal shrink along the Pampean plains was controlled by a decrease in regional precipitation (Fig. 9d). As a consequence, the geochemical signature of higher alkalinity/salinity, marked by higher PC 2 values in the sediments, allows inferring the development of a shallow to intermediate (L1-L2) saline lake during this period (Fig. 9b).

By the 1970s, shallow lakes across the humid pampas started to expand (Piovano et al., 2009; Fig. 9d and e). Reduced lake-water salinities were registered in sediments from Melincué by reduced authigenic carbonate precipitation (Fig. 9b) and relatively deeper and subsaline lake environments (Fig. 9e–g). Sedimentation in a distal area could have reduced the particle size in the deepest part of the lake (Fig. 5). Alike the Melincué lake record, Pampean lake sedimentary archives store an uppermost organic-rich facies corresponding to the post-1970 high-lake level condition (Córdoba et al., 2014; Coianiz et al., 2015; Guerra et al., 2015). Although short-term dry phases triggered in lake-level drops by late 1990s, the water level remained relatively high (L2-L3) until AD 2003, when the highest historical and instrumental level was reached not only in Melincué lake (L3; Fig. 9d) but in all Pampean lakes. This humid period between middle 1970s and 2003 (Fig. 9c) concurred with important precipitation and river-discharge increases along southeastern South America (Camilloni and Barros, 2003; Pasquini et al., 2006; Piovano et al., 2009). Pampean lakes have shown a decreasing water-level trend associated to diminished regional precipitations values, interrupted by a generalized precipitation increase and lake water level rise after 2014 that is still present (Piovano et al., 2014).

Along the CWP, most of the high lake-level pulses caused by positive RPIs and PC 2 decreases in the lacustrine sedimentary record (Fig. 9a, b and c), such as those occurred at ~AD 1878, ~AD 1976, and ~AD 1997, matched strong El Niño phases (i.e. positive El Niño 3.4 pulses; Fig. 9g) . On the other side, positive SST anomalies in the Western Atlantic have become more recurrent during the last 50 years (Tierney et al., 2015) coinciding with the positive RPIs and the development of inter-medium to high lake levels (L2-L3) in Melincué and Mar Chiquita lakes.

Please cite this article in press as: Guerra, L., et al., Climate change evidences from the end of the Little Ice Age to the Current Warm Period registered by Melincué Lake (Northern Pampas, Argentina), Quaternary International (2016), http://dx.doi.org/10.1016/j.quaint.2016.06.033

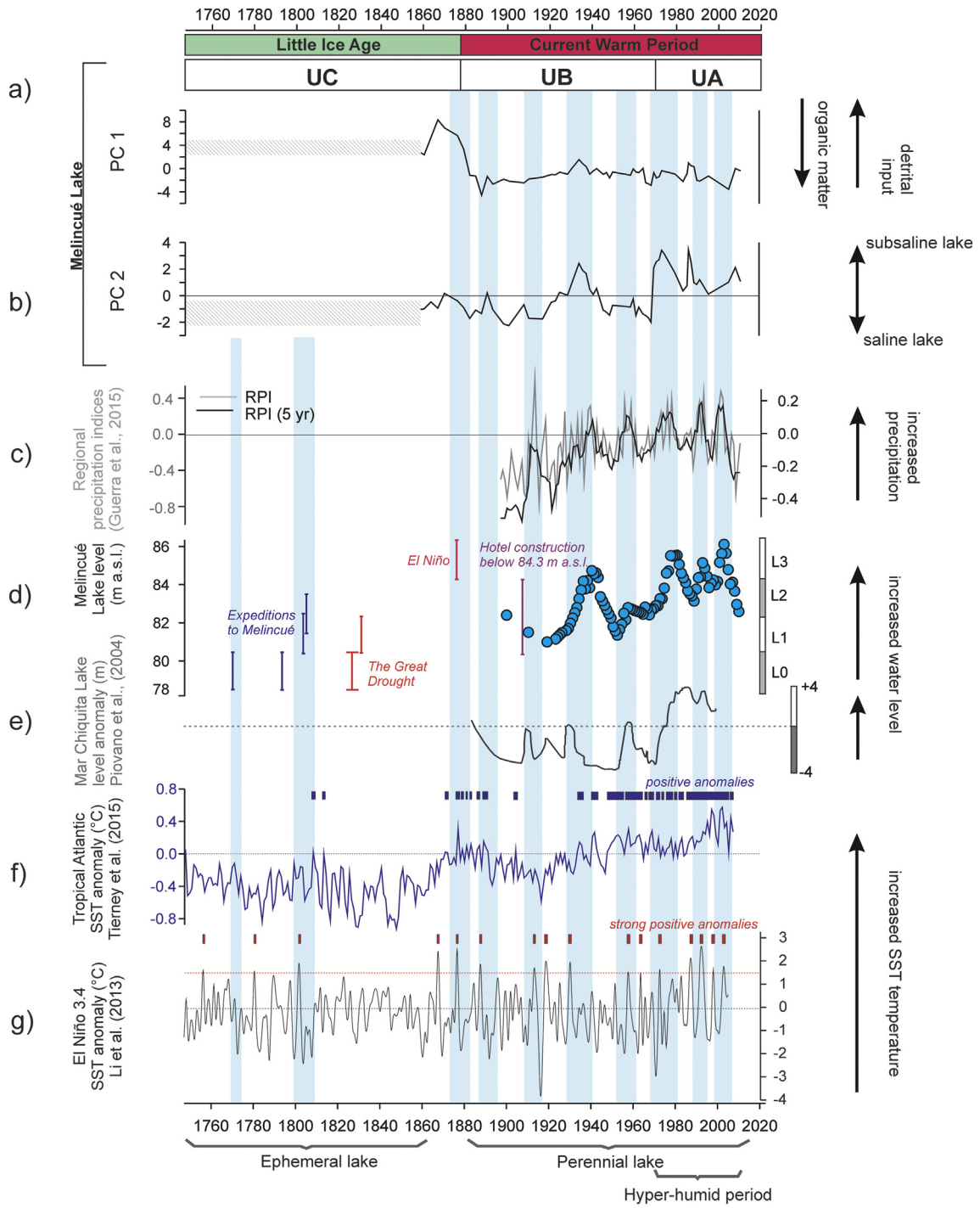

Fig. 9. Paleoclimatic reconstruction from AD 1750 to the present, highlighting the end of the Little Ice Age and the Current Warm Period evolution. **a)** PC 1 variation. **b)** PC 2 variation. A continuous sedimentation model is absent for proxies dating before AD 1860; probable hiatus are highlighted with a diagonal line pattern in a and b. **c)** Regional precipitation index (grey line) and 5-year smoothed regional precipitation index (black line) for Melincué area (Guerra et al., 2015). **d)** Instrumental lake level reconstruction gathered from Melincué (circles, Pasotti et al., 1984; Biasatti et al., 1999; Guerra, 2015). The right axis indicate the relative water lake levels (L0; L1; L2; L3) inferred from the instrumental and historical data (vertical lines): L0 (very shallow to ephemeral); L1 (shallow); L2 (intermediate); L3 (deep). **e)** Mar Chiquita lake level variation (Piovano et al., 2002). **f)** Reconstructions of the sea surface temperature anomalies in the Western Atlantic Ocean from Tierney et al. (2015). The bars correspond to positive SST anomalies. **g)** Extended El Niño 3.4 anomalies over the Pacific Ocean (Li et al., 2013). The lines mark strong positive SST anomalies (anomalies above 1.5). The vertical shadows across the figure highlight the wet periods marked by positive RPI and historical information.

The herein proposed reconstruction agrees with former observations on the climate dynamics that postulate large-scale coupled oceanic-atmospheric changes in the Atlantic or the Pacific oceans as regulating the South American Monsoon dynamics and thus, the moisture flux to the subtropical plains of southeastern South America (e.g. Grimm et al., 2000; Vera et al., 2006; Garreaud et al., 2009). In this way, our results support that reduced rainfall periods (as during the LIA period) and thus low water-levels in Melincué Lake could be the result of a weaker SALLJ humidity transport to the subtropics, matching negative SST

Please cite this article in press as: Guerra, L., et al., Climate change evidences from the end of the Little Ice Age to the Current Warm Period registered by Melincué Lake (Northern Pampas, Argentina), Quaternary International (2016), http://dx.doi.org/10.1016/j.quaint.2016.06.033

anomalies in the Atlantic Ocean, and less intense El Niño episodes. On the contrary, humid conditions, (like the extremely wet phase occurred in the 1970s) could be linked to an enhanced moisture transport to the Pampas through the SALLJ likely forced by more frequent positive SST anomalies in the tropical Atlantic and strong positive anomalies in the Pacific.

7. Conclusions

The sedimentary record of Melincué Lake provides a comprehensive view of the environmental and climatic processes affecting the Pampas along the last five centuries, and gives the opportunity to explore the interaction between climatic forcing factors that rule the hydrological balance in central Argentina. The paleolimnological reconstruction allows deciphering the climate-related environmental changes occurred in the Pampas since ~AD 1492, with decadal resolution in the CWP. The analyses revealed significant sedimentation contrasts between the end of the LIA and the CWP. Shallow and ephemeral lake conditions with extended subaerial lake-floor exposures are inferred for the LIA. This situation is supported by historical sources. Following the LIA, the paleolimnological record revealed a major environmental change by the settlement of a perennial lake by the end of the 19th century, extending during the CWP. The last 40 years of the record since the 1970s refer to dominant deep and subsaline lake conditions triggered by humid regional climate.

The integrated analysis of multiple paleoclimatic reconstructions attests that reconstructed hydroclimate changes which in turn control environmental oscillations registered in Melincué sediments, can be linked to large-scale climatic changes on the Atlantic and Pacific oceans, which regulate the moisture influx to the Pampas through the South American Low Level Jet streams. Evidences suggest synchronic lower SST in the Atlantic and dry conditions in the Pampas during the last part of the LIA, while positive SST anomalies on both oceans agree with wet pulses along the 20th century and the humid period in the Pampas since the 1970s. The obtained results highlight the value of the shallow Pampean lake systems as sensors of regional hydroclimatic changes associated to the South American Monsoon activity during the end of the Little Ice Age and the Current Warm Period.

This study allows a better understanding of the hydrological response of the Pampean lacustrine systems under climatic change scenarios. Further studies on the frequency of local rainfall oscillations would allow planning sustainable development strategies in vulnerable lake-shore communities along the Pampean Plain.

Acknowledgements

The research was supported by a Doctoral Grant from CONICET (Lucía Guerra). The results presented here have been carried out at CICTERRA (CONICET/Universidad de Córdoba, Argentina) and CEREGE (Centre Européen de Recherche et d'Enseignement des Géosciences de l'Environnement, Aix en Provence, France). This study was partially funded by CONICET (PIP 2012-2014/11220110100759), FonCyT (PICT 2013-1371), ECOS SECyT European Community's Seventh Framework Programme (FP7/2007-2013) under Grant Agreement Nº 212492: CLARIS LPB, "A Europe-South America Network for Climate Change Assessment and Impact Studies in La Plata Basin". Our sincere gratitude is always to the firemen from the "Asociación de Bomberos Voluntarios" from Melincué for their selfless help in the field work and core extraction. We appreciate the contributions and comments from the anonymous reviewers and editors that helped to improve the original manuscript.

Appendix A. Supplementary data

Supplementary data related to this article can be found at http://dx.doi.org/10.1016/j.quaint.2016.06.033.

References

Aceituno, P., Prieto, M.R., Solari, M.E., Martínez, A., Poveda, G., Falvey, M., 2009. The 1877–1878 el Niño episode: associated impacts in South Smerica. Climatic Change 92 (3–4), 389–416.
Appleby, P.G., 2008. Three decades of dating recent sediments by fallout radionuclides: a review. The Holocene 18 (1), 83–93.
Aravena, J.C., Luckman, B., 2009. Rainfall of southern South America. International Journal of Climatology 29, 2106–2120.
Azara, F., 1837. Diario de un reconocimiento de las guardias y fortines, que guarnecen la línea de frontera de Buenos-Aires para ensancharla. Imprenta del Estado, Buenos Aires, p. 49.
Biasatti, N., Delannoy, L., Peralta, E., Pire, E., Romano, M., Torres, G., 1999. Cuenca Hidrográfica del Humedal de la Laguna Melincué, Provincia de Santa Fe. ProDIA, SRNyDS, Buenos Aires.
Binford, M.W., 1990. Calculation and uncertainty analysis of ^{210}Pb dates for PIRLA project lake sediment cores. Journal of Paleolimnology 3 (3), 253–267.
Bird, B.W., Abbott, M.B., Vuille, M., Rodbell, D.T., Stansell, N.D., Rosenmeier, M.F., 2011. A 2,300-year-long annually resolved record of the South American summer monsoon from the Peruvian Andes. Proceedings of the National Academy of Sciences 108 (21), 8583–8588.
Boës, X., Rydberg, J., Martinez-Cortizas, A., Bindler, R., Renberg, I., 2011. Evaluation of conservative lithogenic elements (Ti, Zr, Al, and Rb) to study anthropogenic element enrichments in lake sediments. Journal of paleolimnology 46 (1), 75–87.
Bradley, R.S., Briffa, K.R., Cole, J., Hughes, M.K., Osborn, T.J., 2003. The Climate of the Last Millennium. En: Paleoclimate, Global Change and the Future. Springer, Berlin, pp. 105–141.
Brown, E.T., 2011. Lake Malawi's response to "megadrought" terminations: sedimentary records of flooding, weathering and erosion. Palaeogeography, Palaeoclimatology, Palaeoecology 303 (1), 120–125.
Brunetto, E., Iriondo, M., Zamboni, L., Gottardi, G., 2010. Quaternary deformation around the Palo Negro area, Pampa Norte, Argentina. Journal of South American Earth Sciences 29 (3), 627–641.
Bruniard, E., 1982. La diagonal árida Argentina: un límite climático real. Revista Geográfica 95, 5–20.
Burnett, A.P., Soreghan, M.J., Scholz, C.A., Brown, E.T., 2011. Tropical East African climate change and its relation to global climate: a record from Lake Tanganyika, Tropical East Africa, over the past 90 kyr. Palaeogeography, Palaeoclimatology, Palaeoecology 303 (1), 155–167.
Camilloni, I.A., Barros, V.R., 2003. Extreme discharge events in the Paraná River and their climate forcing. Journal of Hydrology 278 (1), 94–106.
Carroll, A.R., Bohacs, K.M., 1999. Stratigraphic classification of ancient lakes: balancing tectonic and climatic controls. Geology 27 (2), 99–102.
Carvalho, L.M., Jones, C., Liebmann, B., 2004. The South Atlantic convergence zone: intensity, form, persistence, and relationships with intraseasonal to interannual activity and extreme rainfall. Journal of Climate 17 (1), 88–108.
Cioccale, M.A., 1999. Climatic fluctuations in the Central Region of Argentina in the last 1000 years. Quaternary International 62 (1), 35–47.
Coianiz, L., Ariztegui, D., Piovano, E.L., Lami, A., Guilizzoni, P., Gerli, S., Waldmann, N., 2015. Environmental change in subtropical South America for the last two millennia as shown by lacustrine pigments. Journal of Paleolimnology 53 (2), 233–250.
Córdoba, F.E., Guerra, L., Cuña Rodríguez, C., Sylvestre, F., Piovano, E.L., 2014. Una visión paleolimnológica de la variabilidad hidroclimática reciente en el centro de Argentina: desde la pequeña edad de hielo al siglo XXI. Latin American journal of sedimentology and basin analysis 21 (2), 0–0.
Croudace, I.W., Rindby, A., Rothwell, R.G., 2006. ITRAX: description and evaluation of a new multi-function X-ray core scanner. Special Publication-Geological Society of London 267, 51.
Dávila, F.M., Lithgow-Bertelloni, C., Giménez, M., 2010. Tectonic and dynamic controls on the topography and subsidence of the Argentine Pampas: the role of the flat slab. Earth and Planetary Science Letters 295 (1), 187–194.
Darwin, C., 1860. A Naturalist's Voyage Round the World, first ed. The Voyage of the Beagle, pp. 142–143. Chapter VII.
Dearing, J., 1994. Environmental Magnetic Susceptibility. Using the Bartington MS2 System. Chi Publishing, Kenilworth, p. 104.
del Puerto, L.D., Bracco, R., Inda, H., Gutiérrez, O., Panario, D., García-Rodríguez, F., 2013. Assessing links between late Holocene climate change and paleolimnological development of Peña Lagoon using opal phytoliths, physical, and geochemical proxies. Quaternary International 287, 89–100.
Deschamps, J.R., Tonni, E.P., 2007. Aspectos ambientales en torno al primer fuerte de la frontera sur de Buenos Aires: "El Zanjón". Universidad de Belgrano, pp. 1745–1779. Documento de Trabajo N° 175. http://www.ub.edu.ar/investigaciones/dt_nuevos/175_deschamps.pdf.
Deschamps, J.R., Otero, O., Tonni, E.P., 2013. Cambio climático en la pampa bonaerense: las precipitaciones desde los siglos XVIII al XX.

Díaz, A., Aceituno, P., 2003. Atmospheric circulation anomalies during episodes of enhanced and reduced convective cloudiness over Uruguay. Journal of climate 16 (19), 3171–3185.
Doyle, M.E., Barros, V.R., 2002. Midsummer low-level circulation and precipitation in subtropical South America and related sea surface temperature anomalies in the South Atlantic. Journal of Climate 15 (23), 3394–3410.
García-Rodríguez, F., Piovano, E., del Puerto, L., Inda, H., Stutz, S., Bracco, R., Panario, D., Córdoba, F., Sylvestre, F., Ariztegui, D., 2009. South American lake paleo-records across the Pampean Region. PAGES News 17 (3).
Garreaud, R.D., Aceituno, P., 2007. Atmospheric Circulation over South America: Mean Features and Variability. The Physical Geography of South America. Oxford University Press, Oxford, England.
Garreaud, R.D., Vuille, M., Compagnucci, R., Marengo, J., 2009. Present-day South American climate. Palaeogeography, Palaeoclimatology, Palaeoecology 281 (3), 180–195.
Gatti, S., 2010. Melincué, su historia. Biblioteca Popular Bernardino Rivadavia, Melincué, Santa Fe, Argentina, p. 100.
Giorgi, F., 2002. Variability and trends of sub-continental scale surface climate in the twentieth century. Part I: Observations. Climate Dynamics 18, 675–691.
Grimm, A.M., Barros, V.R., Doyle, M.E., 2000. Climate variability in southern South America associated with el Niño and La Niña events. Journal of climate 13 (1), 35–58.
Guerra, L., 2015. Registros de la variabilidad hidroclimática del Holoceno tardío en la Llanura Pampeana Argentina: Limnogeología de la laguna Melincué. University of Córdoba, Argentina, p. 222. Ph.D. Thesis.
Guerra, L., Piovano, E.L., Córdoba, F.E., Sylvestre, F., Damatto, S., 2015. The hydrological and environmental evolution of shallow Lake Melincué, central Argentinean Pampas, during the last millennium. Journal of Hydrology 509 (2), 570–583.
Hammer, Ø., Harper, D.A.T., Ryan, P.D., 2001. Past: paleontological statistics software package for education and data analysis. Palaeontologia Electronica 4 (1), 4–9, 178kb. http://palaeo-electronica.org/2001_1/past/issue1_01.htm.
Haberzettl, T., Corbella, H., Fey, M., Janssen, S., Lücke, A., Mayr, C., Ohlendorf, C., Schaebitz, F., Schleser, G.H., Wille, M., Wulf, S., Zolitschka, B., 2007. Lateglacial and Holocene wet-dry cycles in southern Patagonia: chronology, sedimentology and geochemistry of a lacustrine record from Laguna Potrok Aike, Argentina. The Holocene 17 (3), 297–310.
Hijmans, R.J., Cameron, S.E., Parra, J.L., Jones, P.G., Jarvis, A., 2005. Very high resolution interpolated climate surfaces for global land areas. International Journal of Climatology 25 (15), 1965–1978.
Hogg, A.G., Hua, Q., Blackwell, P.G., Niu, M., Buck, C.E., Guilderson, T.P., Heaton, T.J., Palmer, J.G., Reimer, P.J., Reimer, R.W., Turney, C.S.M., Zimmerman, S.R., 2013. Shcal13 southern hemisphere calibration, 0-50,000 years Cal BP. Radiocarbon 55 (4), 1889–1903.
Iriondo, M., Kröhling, D.M., 1995. El sistema eólico pampeano. Museo Provincial de Ciencias Naturales "Florentino Ameghino".
Iriondo, M., Kröhling, D., 2007. Geomorfología y sedimentología de la cuenca superior del río Salado (sur de Santa Fe y noroeste de Buenos Aires, Argentina). Latin American journal of sedimentology and basin analysis 14 (1), 1–23.
Iriondo, M., Brunetto, E., Kröhling, D., 2009. Historical climatic extremes as indicators for typical scenarios of Holocene climatic periods in the Pampean plain. Palaeogeography, Palaeoclimatology. Palaeoecology 283 (3), 107–119.
Jones, P.D., Mann, M.E., 2004. Climate over past millennia. Reviews of Geophysics 42 (2). http://dx.doi.org/10.1029/2003RG000143.
Jones, P.D., Hulme, M., 1996. Calculating regional climatic time series for temperature and precipitation: methods and illustrations. International journal of climatology 16 (4), 361–377.
Kemp, R.A., Toms, P.S., King, M., Kröhling, D.M., 2004. The pedosedimentary evolution and chronology of Tortugas, a Late Quaternary type-site of the northern Pampa, Argentina. Quaternary International 114 (1), 101–112.
Kröhling, D.M., 1999. Upper quaternary geology of the lower Carcarañá Basin, North Pampa, Argentina. Quaternary International 57, 135–148.
Kröhling, D.M., Iriondo, M., 1999. Upper quaternary palaeoclimates of the Mar Chiquita area, North Pampa, Argentina. Quaternary International 57, 149–163.
Kröhling, D.M., Orfeo, O., 2002. Sedimentología de unidades loéssicas (Pleistoceno tardío-Holoceno) del centro-sur de Santa Fe. Revista de la Asociación Argentina de Sedimentología 9 (2), 135–154.
Laprida, C., Orgeira, M.J., García Chapori, N., 2009. El registro de la Pequeña Edad de Hielo en lagunas pampeanas. Revista de la Asociación Geológica Argentina 65 (4), 603–611.
Laprida, C., Valero-Garcés, B., 2009. Cambios ambientales de épocas históricas en la pampa bonaerense en base a ostrácodos: historia hidrológica de la laguna de Chascomús. Ameghiniana 46 (1), 95–112.
Laprida, C., Plastani, M.S., Irurzún, A., Gogorza, C., Navas, A.M., Valero-Garcés, B., Sinito, A.M., 2014a. Mid-late Holocene Lake Levels and Trophic States of a Shallow Lake from the Southern Pampa Plain. Journal of Limnology, Argentina. http://dx.doi.org/10.4081/jlimnol.2014.830.
Laprida, C., Massaferro, J., Mercau, R., Josefina, M., Cusminsky, G., 2014b. Paleobioindicadores del fin del mundo: ostrácodos y quironómidos del extremo sur de Sudamérica en ambientes lacustres cuaternarios. Latin American journal of sedimentology and basin analysis 21 (2), 0–0.
Last, W.M., Ginn, F.M., 2005. Saline systems of the Great Plains of western Canada: an overview of the limnogeology and paleolimnology. Saline Systems 1 (1), 10.
Leroy, S.A.G., Warny, S., Lahijani, H., Piovano, E.L., Fanetti, D., Berger, A.R., 2010. The Role of Geosciences in the Mitigation of Natural Disasters: Five Case Studies. Springer, Netherlands, pp. 115–147.
Li, J., Xie, S.P., Cook, E.R., Morales, M.S., Christie, D.A., Johnson, N.C., Chen, F., D'Arrigo, R., Fowler, A.M., Gou, X., Fang, K., 2013. El Niño modulations over the past seven centuries. Nature Climate Change 3 (9), 822–826.
Mann, M.E., Zhang, Z., Rutherford, S., Bradley, R.S., Hughes, M.K., Shindell, D., Ammann, C., Faluveg, G., Ni, F., 2009. Global signatures and dynamical origins of the Little Ice Age and medieval climate anomaly. Science 326 (5957), 1256–1260.
Martín-Puertas, C., Valero-Garcés, B.L., Mata, M.P., Moreno, A., Giralt, S., Martínez-Ruiz, F., Jiménez-Espejo, F., 2011. Geochemical processes in a Mediterranean Lake: a high-resolution study of the last 4,000 years in Zonar Lake, southern Spain. Journal of Paleolimnology 46 (3), 405–421.
McGregor, H.V., Evans, M.N., Goosse, H., Leduc, G., Martrat, B., Addison, J.A., Mortyn, P.G., Oppo, D.W., Seidenkrantz, M.-S., Sicre, M.-A., Phipps, S.J., Selvaraj, K., Thirumalai, K., Filipsson, H.L., Ersek, V., 2015. Robust global ocean cooling trend for the pre-industrial Common Era. Nature Geoscience 8, 671–678. http://dx.doi.org/10.1038/NGEO2510.
Meyers, P.A., 1994. Preservation of elemental and isotopic source identification of sedimentary organic matter. Chemical Geology 114 (3), 289–302.
Meyers, P.A., 2003. Applications of organic geochemistry to paleolimnological reconstructions: a summary of examples from the Laurentian Great Lakes. Organic geochemistry 34 (2), 261–289.
Neukom, R., Luterbacher, J., Villalba, R., Kuttel, M., Frank, D., Jones, P.D., Grosjean, M., Wanner, H., Aravena, J.C., Black, D.E., Christie, D.A., D'Arrigo, R., Lara, A., Morales, M., Soliz-Gamboa, C., Srur, A., Urrutia, R., von Gunten, L., 2011. Multiproxy summer and winter surface air temperature field reconstructions for southern South America covering the past centuries. Climate Dynamic 37 (1–2), 35–51. http://dx.doi.org/10.1007/s00382-010-0793-3.
Neukom, R., Gergis, J., Karoly, D.J., Wanner, H., Curran, M., Elbert, J., González-Rouco, F., Linsley, B.K., Moy, A.D., Mundo, I., Raible, C.C., Steig, E.J., van Ommen, T., Vance, T., Villalba, R., Zinke, J., Frank, D., 2014. Inter-hemispheric temperature variability over the past millennium. Nature Climate Change 4 (5), 362–367.
Nogués-Paegle, J.N., Mo, K.C., 2002. Linkages between summer rainfall variability over South America and sea surface temperature anomalies. Journal of Climate 15 (12), 1389–1407.
PAGES 2k Consortium, 2013. Continental-scale temperature variability during the past two millennia. Nature Geoscience 6, 339–346.
Pasotti, P., Albert, O.A., Canoba, C.A., 1984. Contribución al conocimiento de la Laguna Melincué. Publicaciones del Instituto de Fisiografía y Geología 66, 1–31.
Pasotti, P., Castellanos, A., 1963. El relieve en la llanura santafesino-cordobesa comprendida entre los paralelos 32° y 33°30S y desde 62°45W hasta el río Paraná. Publicaciones del Instituto de Fisiografía y Geología 47, 1–79.
Pasquini, A.I., Lecomte, K.L., Piovano, E.L., Depetris, P.J., 2006. Recent rainfall and runoff variability in central Argentina. Quaternary International 158 (1), 127–139.
Pavón, P.P., 1969. Diario del P. Pedro Pablo Pavón, 12 de octubre de 1772. In: En De Angelis, P. (Ed.), Colección de obras y documentos IV. Plus Ultra, Buenos Aires, pp. 145–163.
Peralta, E., Romano, M., Delannoy, L., Biasatti, N.R., 2001. Manejo integrado de cuencas hidrográficas. Caso de estudio: La laguna Melincué, Problemática y Perspectivas. Ambiental 4, 90–105.
Piovano, E.L., Ariztegui, D., Moreira, S.D., 2002. Recent environmental changes in Laguna Mar Chiquita (central Argentina): a sedimentary model for a highly variable saline lake. Sedimentology 49 (6), 1371–1384.
Piovano, E.L., Ariztegui, D., Bernasconi, S.M., McKenzie, J.A., 2004. Stable isotopic record of hydrological changes in subtropical Laguna Mar Chiquita (Argentina) over the last 230 years. The Holocene 14 (4), 525–535.
Piovano, E.L., Ariztegui, D., Córdoba, F., Cioccale, M., Sylvestre, F., 2009. Hydrological variability in South America below the tropic of Capricorn (Pampas and eastern Patagonia, Argentina) during the last 13.0 ka. In: En, Vimeux F., Sylvestre, F., Khodri, M. (Eds.), Past Climate Variability from the Last Glacial Maximum to the Holocene in South America and Surrounding Regions: from the Last Glacial Maximum to the Holocene. Springer, pp. 323–351.
Piovano, E.L., Córdoba, F.E., Stutz, S., 2014. Limnogeology in Southern South America: an overview. Latin American Journal of Sedimentology and Basin Analysis 21 (2), 65–75.
Prieto, M.D.R., García Herrera, R., 2009. Documentary sources from South America: potential for climate reconstruction. Palaeogeography, Palaeoclimatology, Palaeoecology 281 (3), 196–209.
Robbins, J., 1978. Geochemical and geophysical applications of radioactive lead. En. In: Nriagu, J.O. (Ed.), The Biogeochemistry of Lead in the Environment, vol. 1A. Elsevier, Amsterdam, pp. 137–184.
Romano, M., Barberis, I., Pagano, F., Maidagan, J., 2005. Seasonal and interannual variation in waterbird abundance and species composition in the Melincué saline lake, Argentina. European Journal of Wildlife Research 51 (1), 1–13.
Sanchez-Cabeza, J.A., Ruiz-Fernández, A.C., 2012. ^{210}Pb sediment radiochronology: an integrated formulation and classification of dating models. Geochimica et Cosmochimica Acta 82, 183–200.
Servicio Geológico Minero Argentino, 1997. Mapa geológico de la República Argentina, escala 1: 2,500,000. Buenos Aires.
Stuiver, M., Reimer, P.J., 1993. Extended ^{14}C data base and revised CALIB 3.0 ^{14}C age calibration program. Radiocarbon 35 (1), 215–230.
Stutz, S., Borel, C.M., Fontana, S.L., Tonello, M.S., 2012. Holocene changes in trophic states of shallow lakes from the Pampa plain of Argentina. The Holocene 22 (11), 1263–1270.

Please cite this article in press as: Guerra, L., et al., Climate change evidences from the end of the Little Ice Age to the Current Warm Period registered by Melincué Lake (Northern Pampas, Argentina), Quaternary International (2016), http://dx.doi.org/10.1016/j.quaint.2016.06.033

ARTICLE IN PRESS

Thompson, R., Clark, R.M., Boulton, G.S., 2012. Core Correlation. In Tracking Environmental Change Using Lake Sediments. Springer, Netherlands, pp. 415–430.
Thompson, L.G., Mosley-Thompson, E., Davis, M.E., Zagorodnov, V.S., Howat, I.M., Mikhalenko, V.N., Lin, P.N., 2013. Annually resolved ice core records of tropical climate variability over the past ~1800 years. Science 340 (6135), 945–950.
Tierney, J.E., Abram, N.J., Anchukaitis, K.J., Evans, M.N., Giry, C., Kilbourne, K.H., Saenger, C.P., Wu, Z., Zinke, J., 2015. Tropical sea surface temperatures for the past four centuries reconstructed from coral archives. Paleoceanography 30 (3), 226–252.
Tonni, E.P., Cione, A.L., Figini, A.J., 1999. Predominance of arid climates indicated by mammals in the pampas of Argentina during the Late Pleistocene and Holocene. Palaeogeography, Palaeoclimatology, Palaeoecology 147 (3), 257–281.
Tripaldi, A., Zárate, M.A., Forman, S.L., Badger, T., Doyle, M.E., Ciccioli, P., 2013. Geological evidence for a drought episode in the western Pampas (Argentina, South America) during the early–mid 20th century. The Holocene 23 (12), 1731–1746.
Troin, M., Vallet-Coulomb, C., Sylvestre, F., Piovano, E., 2010. Hydrological modelling of a closed lake (Laguna Mar Chiquita, Argentina) in the context of 20th century climatic changes. Journal of Hydrology 393 (3), 233–244.
Troin, M., Vrac, M., Khodri, M., Caya, D., Vallet-Coulomb, C., Piovano, E., Sylvestre, F., 2015. A complete hydro-climate model chain to investigate the influence of sea surface temperature on recent hydroclimatic variability in subtropical South America (Laguna Mar Chiquita, Argentina). Climate Dynamics 1–16.
Vera, C., Higgins, W., Amador, J., Ambrizzi, T., Garreaud, R., Gochis, D., Gutzler, D., Lettenmainer, D., Marengo, J., Mechoso, C.R., Nogués-Paegle, J., Silva Dias, P.L., Zhang, C., 2006. Toward a unified view of the American monsoon system. Journal of Climate 19, 4977–5000.
Villalba, R., 1994. Tree-ring and glacial evidence for the medieval Warm epoch and the Little ice age in southern South America. In: The Medieval Warm Period. Springer, Netherlands, pp. 183–197.
Vuille, M., Burns, S.J., Taylor, B.L., Cruz, F.W., Bird, B.W., Abbott, M.B., Kanner, L.C., Cheng, H., Novello, V.F., 2012. A review of the South American monsoon history as recorded in stable isotopic proxies over the past two millennia. Climate of the Past 8 (4), 1309–1321.
Warren, J.K., 2010. Evaporites through time: tectonic, climatic and eustatic controls in marine and nonmarine deposits. Earth-Science Reviews 98 (3), 217–268.
Zanor, G.A., Piovano, E.L., Ariztegui, D., Vallet-Coulomb, C., 2012. A modern subtropical playa complex: salina de Ambargasta, central Argentina. Journal of South American Earth Sciences 35, 10–26.
Zárate, M.A., 2003. Loess of southern South America. Quaternary Science Reviews 22, 1987–2006.
Zhou, J., Lau, K.M., 1998. Does a monsoon climate exist over South America? Journal of Climate 11, 1020–1040.
Zhou, J., Lau, K.M., 2001. Principal modes of interannual and decadal variability of summer rainfall over South America. International Journal of Climatology 21 (13), 1623–1644.

Please cite this article in press as: Guerra, L., et al., Climate change evidences from the end of the Little Ice Age to the Current Warm Period registered by Melincué Lake (Northern Pampas, Argentina), Quaternary International (2016), http://dx.doi.org/10.1016/j.quaint.2016.06.033